Design Optimization Studies of Partially Superconducting Machines based on NASA's High Efficiency Megawatt Motor

Thomas F. Tallerico[1], Aaron D. Anderson[2], and Justin J. Scheidler[3]
NASA Glenn Research Center, Cleveland, OH, 44135, USA

Single aisle class electric aircraft require high power density and efficient megawatt-scale electric machines to be competitive with their traditional turbofan counterparts. Superconducting machines are seen as a key enabling technology for achieving the electric motor power density and efficiency needed by these aircraft. NASA's High Efficiency Megawatt Motor (HEMM) is a partially superconducting machine being developed at NASA Glenn Research Center as a technology demonstration of a practical near-term superconducting machine. HEMM is being developed to meet the requirements of the generators on NASA's STARC-ABL reference aircraft. HEMM is expected to achieve greater than 16 kW/kg electromagnetic specific power and greater than 98% efficiency at a nominal operating condition of 1.4 MW and 6800 RPM. In this paper, a design optimization algorithm for partially superconducting machines based on HEMM's technologies is used to explore the possible performance of HEMM technology at other machine power levels and operating conditions. The design optimization algorithm is detailed in full, and results for achievable geared and direct drive machine performance are presented.

I. Nomenclature

A	=	Electrical Loading
a	=	area
ag	=	airgap
B	=	magnetic flux density
d	=	wire diameter
D	=	Diameter
E	=	Efficiency
f	=	frequency
h	=	convective heat transfer coefficient
k	=	thermal conductivity
L	=	Length
M	=	Mass
P	=	Power
r	=	radius
R	=	reluctance or resistance
RPM	=	rotational speed in rev's per min
t	=	time
$t_{winding}$	=	winding thickness
T	=	time period of magnetic flux repetition
w	=	width
V	=	volume
α	=	Steinmetz frequency coefficient
β	=	Steinmetz flux density coefficient
γ	=	Steinmetz Coefficient
γ_1	=	Modified Steinmetz Coefficient
ρ	=	resistivity of magnet material
σ	=	electrical conductivity
τ	=	Torque
ω	=	rotation speed

[1] Research Aerospace Engineer, Rotating and Drive Systems Branch, thomas.tallerico@nasa.gov.
[2] Electrical Engineer, Diagnostics and Electromagnetics Branch, aaron.d.anderson-1@nasa.gov.
[3] Research Mechanical Engineer, Rotating and Drive Systems Branch, justin.j.scheidler@nasa.gov.

II. Introduction

Single aisle class electric or hybrid electric aircrafts require megawatt class motors with high efficiency and specific power to become practical alternatives to traditional aircraft. Partially and fully superconducting electric motors are viewed as key enabling technologies in this design space [1] [2]. As such, a number of papers have been written on designs and design studies of superconducting machines for electric aircraft in recent years [3] [4] [5] [6]. NASA's main contribution to the exploration of this design space has been the development of its High Efficiency Megawatt Motor [7] [8] [9] [10] [11] [12] [13] [14] [15].

NASA's High Efficiency Megawatt Motor (HEMM) is a 1.4-megawatt wound field partially superconducting synchronous machine. HEMM has been specifically developed to meet the requirements of the two generators on NASA's STARC-ABL reference vehicle [16]. It has performance targets of greater than 16 kW/kg electromagnetic specific power and greater than 98% efficiency at a nominal rotational speed of 6800 RPM. Those performance targets are however only relevant to the selected design point and are not representative of what could be achieved using HEMM technology in other applications.

In this paper, a design optimization tool is used to explore what machine performance can be achieved using HEMM technology at other powers in both direct drive and geared drivetrains. Section III of this paper presents the developed design optimization tool. Section IV presents design study results for motor performance in both geared and direct drive cases. Conclusions are summarized in Section V.

III. Design Optimization Tool

The developed optimization tool uses a combination of analytical equations and 2D finite element electromagnetic analysis to predict the achievable electromagnetic efficiency of HEMM technology across a range of power and specific power levels for a given set of constraints. A genetic optimization algorithm is used to sequentially complete both analytical and finite element analysis (FEA) based optimizations of motor electromagnetic geometries. In both cases, the design tool is written to extract as much information as possible from a single electromagnetic analysis of a 2D motor geometry. The results of each 2D analysis are used to predict the performance of machines that have that 2D electromagnetic geometry at multiple power levels, specific powers, and rotational speeds. The flow diagram in Figure 1 shows the design tool workflow.

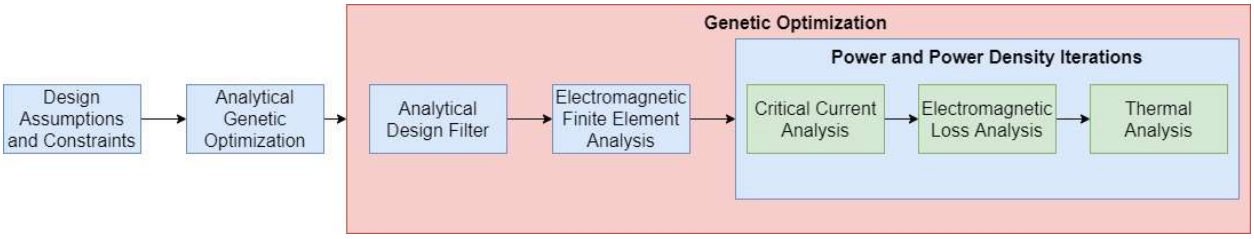

Figure 1 Design Algorithm Flow Diagram

As seen in the flow diagram, the optimization starts by inputting the desired operating conditions and constraints into a fully analytical genetic optimization. The assumptions and constraints used in this paper's design studies are given in Section III-A. The analytical algorithm's magnetic model is presented in section III-B. The results of the fully analytical genetic optimization are used to down select the design space for the FEA based genetic optimization and reduce the overall computational cost of the entire optimization.

The FEA-based optimization uses the fully analytical analysis tool as a filter to eliminate 2D geometries selected by the genetic optimizer for which no good machine design exists. If a design passes the analytical filter, 2D finite element analysis is used to evaluate the superconducting coil critical current, motor torque, and electromagnetic loss characteristics of that 2D geometry. Parametric sweeps of rotor current and stator current are run in the 2D FEA. The output of a 2D electromagnetic FEA analysis is multiple interpolation functions for the superconducting coils' critical current, motor torque, and electromagnetic losses as a function of rotor current, stator current, and the machine stack length for the analyzed 2D geometry. The interpolation functions are used to predict the efficiency of machines that have that 2D geometry at multiple pre-selected power levels, specific powers, and rotational speeds. The details of how this is done are described in Section III-D.

The result of each analysis (either analytical or FEA) is a vector of efficiencies for machines that use the analyzed 2D electromagnetic geometry at different power levels and specific powers. This vector is used as the fitness of the

geometry, and a multi-objective optimization is carried out to optimize efficiency for each preselected combination of power and specific power.

A. Design Tool Assumptions

Table 1 summarizes the key assumptions in the design tool. All assumptions are based on the HEMM design. The basic magnetic geometry of the motor topology is depicted in Figure 2.

Table 1 Design Code Assumptions

Bus Voltage	1200 V	**Magnetic Airgap**	6.5 mm
Phases	9	**Rotor Temperature**	62 K
Stator Winding	Form Wound Air Core	**Superconductor**	2G REBCO
Back Iron Material	$Fe_{49.15}Co_{48.75}V_2$ (0.1 mm)	**S.C. Tape Width**	4 mm
Winding Material	Copper	**S.C. Tape Thickness**	65 um
Strand Insulation	MW-16 Polyimide	**Coil Type**	4-layer Pancake
Turn Insulation	Nomex	**Coil Fill**	90%
Potting Epoxy Thermal Conductivity	1.5 W/(m*K)	**Rotor Iron**	$Fe_{49.15}Co_{48.75}V_2$ (no laminations)
Coolant Temp	60 ˚C	**Max Winding Temp**	200 ˚C

A bus voltage of 1200 volts is assumed in order to define the required insulation thicknesses in the stator windings. The stator windings are assumed to be composed of litz wire to minimize winding AC resistive and proximity losses in the high field produced by the superconducting rotor. The strand insulation is assumed to be polyimide while the turn insulation is assumed to be a Nomex over wrap. A high thermal conductivity epoxy is assumed for the potting compound. HEMM's insulation system, discussed in [17], is the basis for the material assumptions and selections here.

A 6.5 mm magnetic airgap is maintained for all the designs, which matches HEMM. In the HEMM design, the 6.5 mm magnetic gap is composed of the physical gap, the rotor vacuum chamber's radial thickness, and the fluid flow gap for stator cooling [11].

The rotor coils are 4-layer pancake coils composed of a second generation REBCO tape. The construction and thermal cycling of these coils for HEMM is discussed in [13] [14]. The assumed operating temperature for the coils is 62 K, the target operating temperature of HEMM's rotor. An interpolation function for the superconducting tape (based on data from the manufacturer) is used to predict the coil's critical current in the design tool based on the magnetic loading and this temperature. The rotor superconducting coil operating current is selected such that the critical current is more than 1.5 times the operating current.

Two mechanical constraints are maintained on all the designs. The first is a simple requirement that the rotor must have a length to diameter ratio of less than 2 to mitigate rotordynamics concerns. The second is a limit on the centripetal loading per stack length of the rotor coil. The superconducting wire are fragile composites and are especially susceptible to delamination of the superconducting layer from its substrate within the wire. To mitigate the risk of mechanical failure of HEMM's superconducting coils, NASA has completed spin testing of the HEMM coil design to show that it survives the expected centripetal loads during motor operation. Since no data exists past this level of centripetal loading for the coils, the requirement is set to keep rotor coil centripetal loads less than the expected level in the HEMM rotor. The limit on centripetal load is set such that each individual rotor coil must produce less than 143 kN of centripetal force per meter axial length. This loading limit is used to constrain the max rotational speed of a given 2D machine geometry in the design tool.

Electrical frequency on all the designs is limited to a max of 1000 Hz to avoid motor designs that would require too high of switching frequency or large inverter filters. Due to HEMM's cryocooler only being able to reject 50 Watts of heat at its operating temperature, HEMM puts significant burden on the inverter driving it to provide low harmonic distortion current to limit the corresponding rotor losses. This requirement becomes more stringent and more difficult to meet as electrical frequency increases. In the future, a combined inverter and motor optimization tool is likely needed to produce an optimum system.

Table 2 lists the six variables used by the genetic algorithm to optimize machine designs. These parameters are used to define the motor geometry as depicted in Figure 2.

Table 2 Design Tool Optimization Variables

Rotor Back Iron Thickness Ratio	Rotor Iron Tooth Width
Stator Back Iron Thickness	Stator Winding Radial Thickness
Rotor Pole Pair Count	Rotor Radius

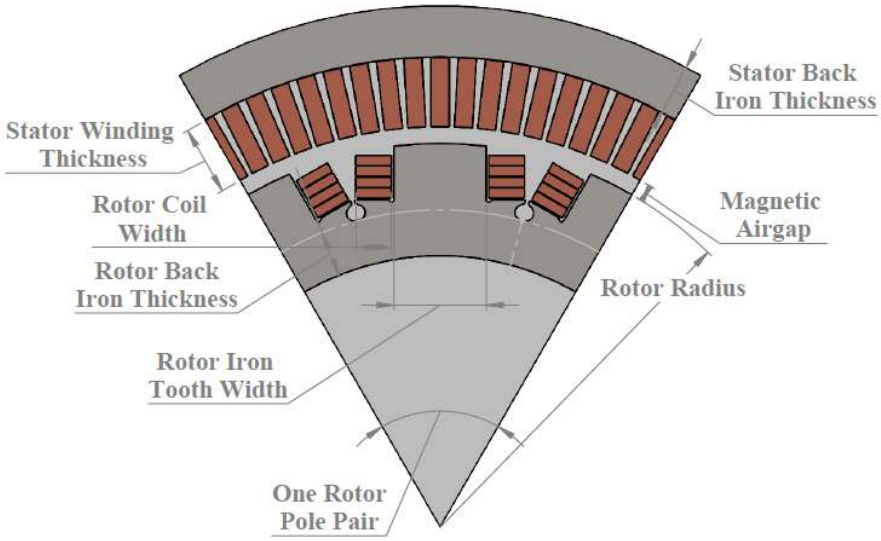

Figure 2 Electromagnetic Geometry Definitions

In Table 2, rotor back iron thickness ratio is defined as rotor back iron thickness divided by rotor iron tooth width. This ratio is used to set the rotor back iron thickness.

Rotor coil geometry is optimized for each design iteration to maximize the number of turns in each coil layer. The coil's structural retention components are accounted for by including 1.5 mm of space around the coil for the titanium coil cup, dovetail retention component, and end winding retaining hoops in the HEMM rotor design [14]. Coil radial position and width are selected to maximize turn count within the available remaining area.

B. Analytical Electromagnetic Model

A low fidelity analytical electromagnetic model is used both to initially down select the design space for the FEA based optimization and then as a filter within the FEA based design optimization. This model breaks the analysis of the motor geometry into two cases: before and after the rotor iron is saturated. In both cases it is assumed that the superconducting rotor produces all the field in the airgap of the machine. The field from the room temperature stator windings is neglected. This assumption is accurate for HEMM, because the amp-turns of its rotor coils are about 40 times greater than that of each stator phase. A simple magnetic reluctance model (Figure 3) is used to evaluate the motor geometries in the pre-rotor iron saturation condition. For the post-saturation case, the rotor coil turns are treated as conductors in air and fields are calculated using the Biot-Savart Law. Both models are used to calculate the peak B field in the stator coils, rotor coils, and the stator back iron. The following two sections discuss each model.

1. Reluctance Network Model

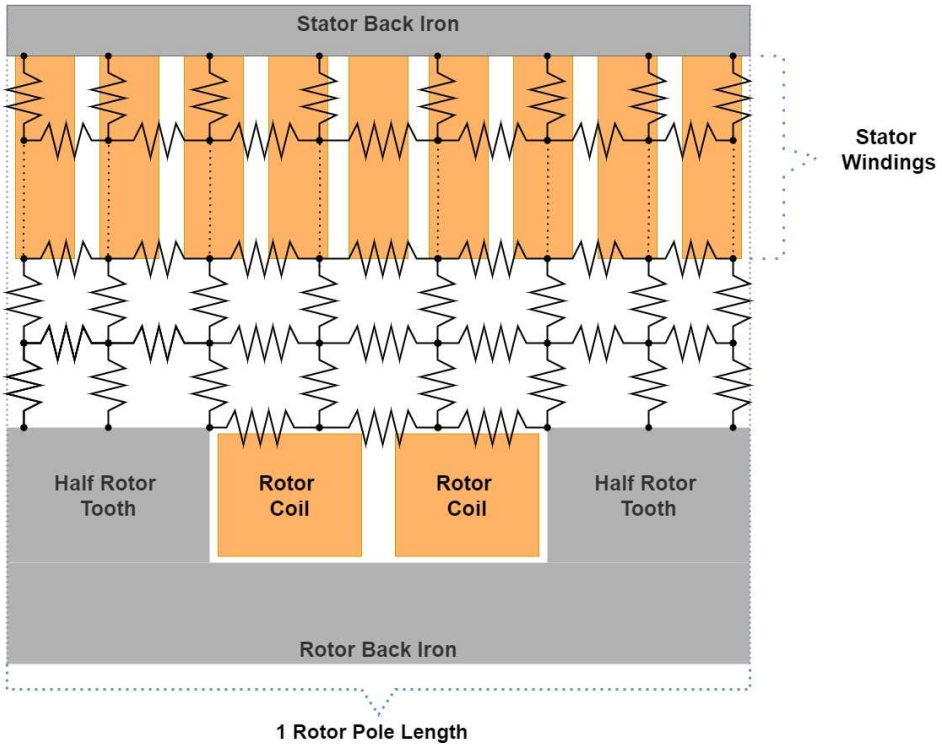

Figure 3 Analytical Reluctance Network Model

The reluctance network model used to evaluate the fields up to the point of rotor saturation is depicted in Figure 3. The model consists of 105 reluctances between 61 nodes. Both the stator back iron and the rotor iron are assumed to be infinitely permeable.

The model is solved assuming flux source conditions at the rotor teeth, where the flux source magnitude is defined by the flux needed to saturate the rotor iron. B field values in the rotor coils, the stator coils, and the stator back iron are calculated. The required number of amp-turns from the rotor coils needed to saturate the rotor iron is calculated and used to define the current in the rotor coils.

The B field in the rotor coil from this model is used to calculate the rotor coil's critical current at the point of rotor iron saturation. A check is carried out to verify that this value is above 1.5 times the current required to saturate the rotor iron. If it is not, the design is de-rated appropriately and the B fields calculated for the stator coils and iron from the reluctance model are used to calculate machine performance as described in Section III-B-3. If the critical current is more than 1.5 times the current needed to saturate the iron, the Biot-Savart Law is used to evaluate the design past the point of rotor iron saturation and determine the rotor current level where critical current is 1.5 times higher than the rotor current.

2. Biot-Savart Law Model

If a given geometry passes through the reluctance model and the critical current condition is not met at the point of rotor saturation, the rotor coil turns are treated as individual wires in air. Fields are calculated using the Biot-Savart Law and superimposed on the fields calculated using the reluctance network. The exact location of each rotor coil turn is defined, and a summation of the fields produced by each individual conductor is used to calculate the additional field after rotor core saturation. An iterative solver is used to find the rotor coil current that results in critical current being 1.5 times the rotor current. This point is defined as the rotor coil's operating current in the analytical model.

With rotor operating current defined, B field values in both the stator coils and back iron are calculated for the additional current past rotor iron saturation using the Biot-Savart Law. The field values are added to those calculated using the reluctance network for the torque and loss calculations described in the following section.

3. Analytical Torque and Loss Calculations

The fields predicted by the analytical model are used to create basic loss and efficiency estimates for machines that use the analyzed 2D geometry. RPM, specific power, and power iterations are carried out as described in Section III-E to define the fitness of the 2D geometry.

For the analytical model in these iterations, stator iron losses per meter of motor stack length are defined using the Stienmetz equation

$$Pperm_{iron} = a_{iron}\rho_{iron}kB_{iron}^{\beta}f^{\alpha} \tag{1}$$

where $Pperm_{iron}$ is the iron loss per meter of motor stack length, a_{iron} is the iron's cross-sectional area, ρ_{iron} is the density of iron, f is electrical frequency, and k, β, and α are the standard Steinmetz coefficients.

For calculating stator winding proximity loss, a proximity loss coefficient is calculated and used in place of the FEA based coefficient described in Appendix A and B. The coefficient is defined as

$$C_{proximity} = \frac{\pi}{12}a_{winding}f^2B_{peak}^2 \tag{2}$$

where $C_{proximity}$ is the proximity loss coefficient, $a_{winding}$ is the total cross-sectional area of each stator winding, and B_{peak} is the peak B field produced by the rotor in the stator windings.

To calculate required stator current in the RPM, power, and specific power iterations, the standard D^2L sizing equation for electric machines is used

$$\tau_{perm} = \frac{P}{\omega} = \sqrt{2}B_{peak}A_{rms}r^2 \tag{3}$$

where τ_{perm} is motor torque per meter of motor stack length, P is power, ω is motor rotation speed, B_{peak} is the peak magnetic field produced by the rotor in the stator windings, A_{rms} is the electrical loading of the stator calculated using root mean squared current, and R is the airgap radius.

4. Analytical Model Performance

The primary flaw in this analytical model is that the stator iron permeability is neglected in the Biot-Savart field calculations. Correspondingly, required stator back iron thickness is underpredicted in the analytical model relative to FEA. This error results in the analytical model predicting lower optimum pole counts than the FEA model. As described in Section IV, this error resulted in needing to run the model for explicit pole counts and is a needed point of improvement in the design tool.

C. Electromagnetic Finite Element Model

The electromagnetic FEA model is used for higher fidelity evaluation of the electromagnetic characteristics of each 2D geometry selected by the genetic optimization. An example FEA geometry and simulation result is shown in Figure 4. The output of each FEA analysis is a set of interpolation functions for the given 2D geometry that define magnetic losses, rotor critical current, and torque as functions of rotor current, stator current, and motor axial length. These interpolation functions are then used to estimate the efficiency of machines with the given 2D geometry at multiple power levels and specific powers as described in Section III-E.

Before each FEA evaluation of a 2D geometry, the analytical model is run to both evaluate if any good machines exist for that 2D geometry and provide estimates of the relevant rotor and stator currents for good machines. The FEA then solves to produce the interpolation functions for machine performance in the range around the analytically predicted relevant current values.

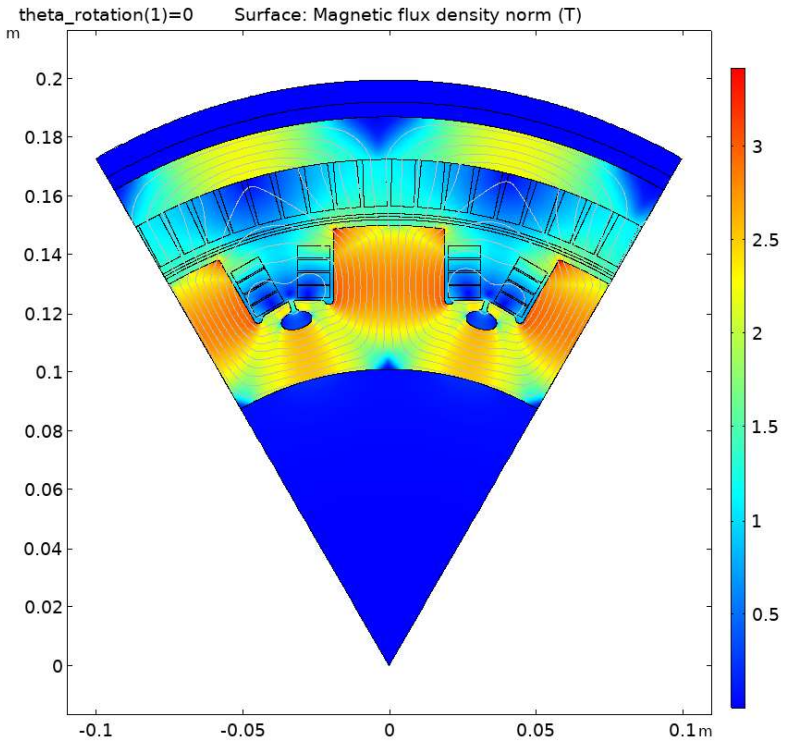

Figure 4 Example electromagnetic FEA simulation result.

The FEA simulations are highly nonlinear because the high number of amp-turns in the superconducting rotor windings drives the rotor iron well past magnetic saturation for most geometries that achieve high efficiency. For the solutions to converge in a reasonable time, a multistep solver configuration with load ramping had to be used to handle the nonlinearity and use appropriate initial conditions for each simulation. The solver configuration used to efficiently solve the FEA current sweeps is depicted in Figure 5. The first step in the configuration is ramping the rotor current to the highest relevant value predicted by the analytical equations. For this step, the stator current is set to the minimum value of interest in the parametric sweep and the rotor current is ramped in 10 A increments from zero to the highest relevant value. The next step is a parametric sweep of stator currents at each relevant rotor current level. The solutions from the rotor current ramp step are used as the initial conditions for the minimum stator current cases. For higher stator current cases, the solution for the next lowest stator current and equal rotor current is used as the initial condition in the solver. This solver configuration ensures that every step has a reasonable initial condition and can converge quickly.

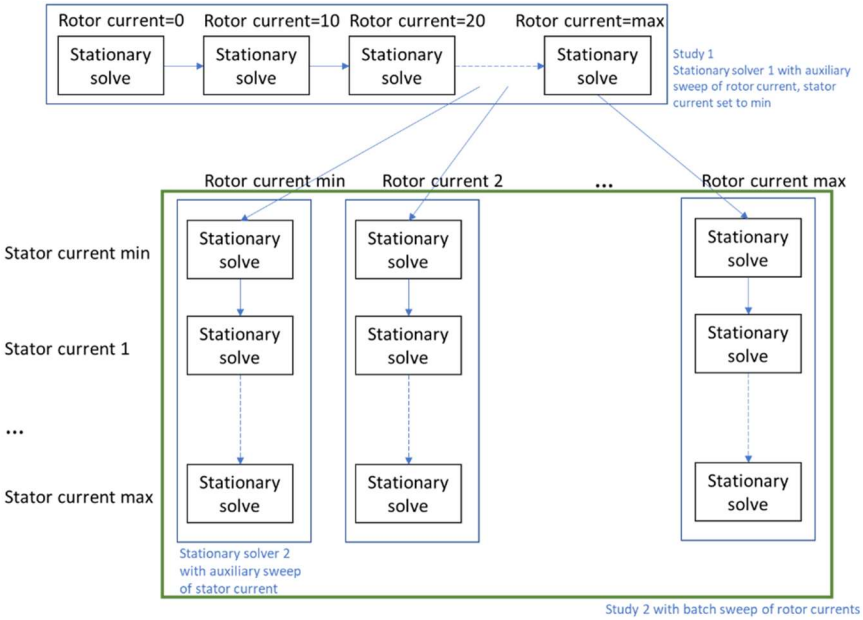

Figure 5 FEA solver configuration

After solving the FEA model for the full range of stator and rotor currents selected by the analytical tool, magnetic field data and the torque produced per meter of motor stack length is output from the FEA model at each combination of rotor current and stator current. Examples of the results pulled from the FEA simulation are shown in Figure 6 and Figure 7. Interpolation functions for magnetic losses per meter of motor stack length, torque per meter of motor stack length, and the rotor coil's critical current are created from the data as functions of rotor and stator current. The calculation of magnetic losses (stator iron and winding proximity) is described in Appendix A. The aforementioned critical current interpolation function is used to determine the allowable combinations of rotor current and stator current for which critical current is more than 1.5 times the rotor current. All the interpolation functions are used in the RPM, power, and specific power iterations to define the fitness of the 2D geometry as described in section III-E.

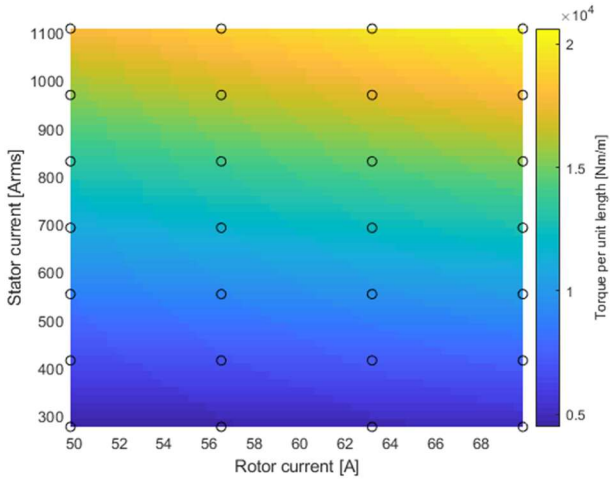

Figure 6 Torque per axial length generated as a function of rotor and stator currents to be used for interpolation. Black circles indicate points calculated by FEA and color indicates interpolated values.

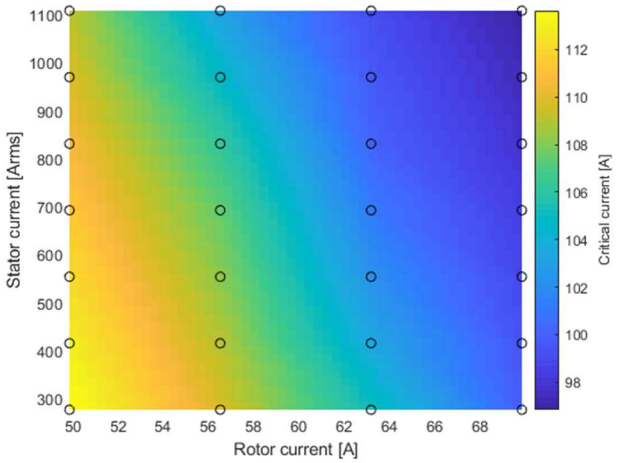

Figure 7 Critical current as a function of rotor and stator currents to be used for interpolation. Black circles indicate points calculated by FEA and color indicates interpolated values.

D. Thermal Model

A simple 1D thermal resistance network model is used to evaluate the thermal performance of every design during the power, specific power, and RPM iterations described in Section III-E. The cooling method is assumed to be the one used in HEMM [11], where 60 ˚C coolant is flowed through the airgap of the machine between the stator windings and the vacuum tube as well as over the back iron of the machine. The primary goal of the thermal model is to eliminate designs that would be impractical or difficult to cool. The thermal resistance network model is shown graphically in Figure 8.

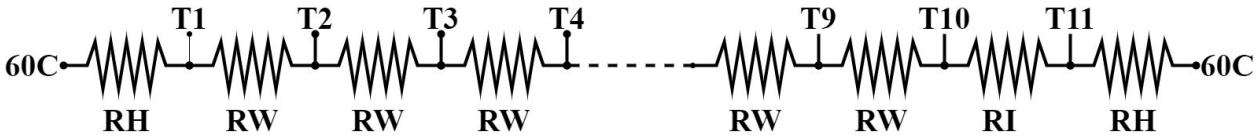

Figure 8 1D Design Tool Stator Thermal Resistance Network Model. RH is the resistance for the convective heat transfer. RW's are the thermal resistance of the winding broken into 10 radial sections. RI is the thermal resistance of the stator iron.

The thermal network model consists of 12 resistances and 13 temperature nodes. The stator winding is broken up into ten temperature nodes (T1-T10) in order to provide some thermal gradient resolution within the stator windings. The thermal resistance between each of these ten nodes is taken to be

$$RW = \frac{t_{winding}}{10 * A * k_{w2}} \tag{6}$$

Where RW is the thermal resistance, A and $t_{winding}$ respectively are the cross-sectional area and radial thickness of the given section of stator winding, and k_{w2} is the winding's radial thermal conductivity, which is defined in Appendix B. A single thermal resistance is used to represent the stator back iron.

For simplicity, the effective convection coefficient of the fluid flow on the inner diameter of the windings and the outer diameter of the stator iron is assumed to be 5000 W/(m^{2}K). This value is meant to represent a reasonable, but high convection coefficient for fluid flow. The model is solved using the 60 ˚C fluid temperature boundary condition and the heat loads predicted either by the FEA or analytical electromagnetic model. Peak winding temperature is predicted by twice iterating the winding analysis described in Appendix B with the thermal resistance analysis. If the predicted winding temperature is above 200 ˚C for a given machine design, that design is assigned an efficiency of zero.

E. Power, Specific Power, and RPM Iterations

For each run of the design tool, whether analytical or FEA based, a set of predefined combinations of power and specific power are set for the code to evaluate achievable machine efficiency for. The fitness of each 2D geometry evaluated in the genetic algorithm is a vector of the maximum efficiency achievable at each desired combination of power and specific power. Within the assumptions and constraints of each design tool run, rotational speed is a free variable that the design tool iterates in 500 RPM increments at each power and specific power level. After each rotational speed is evaluated for a given combination of power and specific power, the optimum rotational speed is selected to maximize efficiency, and the corresponding efficiency value is used in the fitness of the 2D geometry. Figure 9 graphically depicts how the power, specific power, and RPM iterations are carried out.

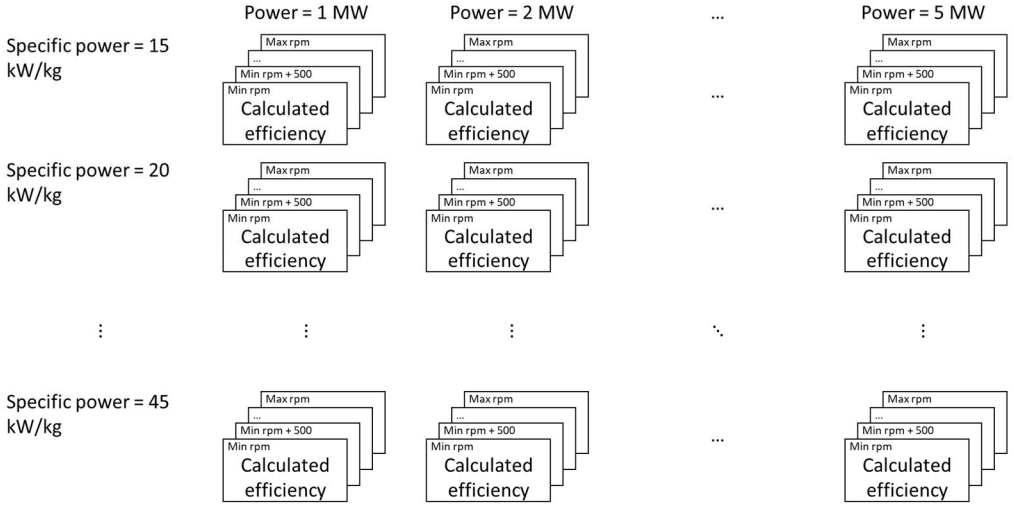

Figure 9 Results from FEA model for one geometry.

To carry out these iterations, at each combination of power and specific power, the mass of the machine is calculated as

$$mass = \frac{Power}{Specific\ power} \tag{4}$$

An appropriate stack length for a given 2D motor geometry can then be calculated by subtracting off the mass of the stator winding and rotor coil end turns and then dividing the remaining mass by the mass per meter of motor stack length calculated for the given 2D geometry. The required torque per meter of stack length can then be calculated at each rotational speed as

$$\tau_{perm} = \frac{Power}{\omega * Stack} \tag{5}$$

The torque per meter of motor stack length interpolation function is then used to determine the combinations of stator current and rotor current that produce the required torque. The stator current and rotor current are fed into the interpolation function for the rotor coil's critical current, and combinations that result in critical current being less than 1.5 times the operating current are eliminated.

With stack length set, stator iron losses and winding proximity loss coefficients can be calculated using the corresponding interpolation functions described in Appendix A at the allowable combinations of required stator current and rotor current. Motor winding analysis (Appendix B) is then carried out to predict winding slot fill, wire gauge, AC resistive losses, proximity losses, and winding thermal properties based on minimizing the combined proximity and AC resistive winding losses at each allowable combination of required stator current and rotor current. A final rotor and stator current combination is then selected based on minimizing combined resistive, proximity, and iron loss to maximize efficiency. The corresponding loss values are then fed to the thermal model described in Section III-D and efficiency is set to zero if the machine design doesn't close thermally. If the machine can close thermally,

two iterations of thermal and winding analysis are completed to increase the convergence between actual winding temperature and winding loss.

For every 2D geometry selected by the genetic optimization and analyzed by either the analytical or FEA electromagnetic model, this calculation is completed for all power, specific power, and rotational speed iterations. Optimum rotational speed is selected for each combination of power and specific power; the corresponding efficiency values are used to define the fitness of the geometry.

IV. Design Optimization Results

For this paper, the design code was executed for two cases: a geared motor case and a direct drive case. For the geared motor case, RPM is a free variable in the design process and the code is run to find the optimum RPM and geometry for each power level and specific power. The rotor coil's centripetal loading condition and the electrical frequency limit described in Section III-A are the only constraint on rotor speed in the geared case.

In the direct drive case, RPM is given a pre-set value of 3000 RPMs (a typical value for aircraft propeller rotational speed). In order to keep sufficient fan area available, a rotor tip speed constraint is applied to limit machine radius. Three different rotor tip speed limits are evaluated: 80, 100, and 120 m/s.

A. Geared Results

For the geared design study, RPM was allowed to vary in 500 rpm increments up to the max allowable speed of a given geometry. The max speed for each geometry was limited by either electrical frequency or the centripetal loading of the superconducting coils. The analytical optimization for the full design space predicted that 6 pole pairs and roughly 10 krpm would be optimum. However, an initial FEA optimization suggested higher pole counts to be optimum. Comparing results of explicit cases run in both the analytical and FEA tool, it was found that the needed stator iron thickness was being underpredicted by the analytical tool and, correspondingly, the analytical tool was favoring lower pole count machines more than it should. As mentioned above, this error in the analytical model is caused by the stator iron's permeability being neglected in the Biot-Savart field calculation. To correct for this error, design tool runs were completed for machine pole counts one at a time for the geared motor study. Table 3 summarizes the design tool runs completed. Figures 10 thru 14 show the results of the design tool runs. The data for the plots is provided in Appendix C.

Table 3 Design cases run for the geared HEMM case

Variable	Values
Power Levels	1:1:5 MW
Electromagnetic Specific Power Levels	15:5:45 kW/kg
Rotor Pole Pairs	6, 8, 10, 12, 16, and 20

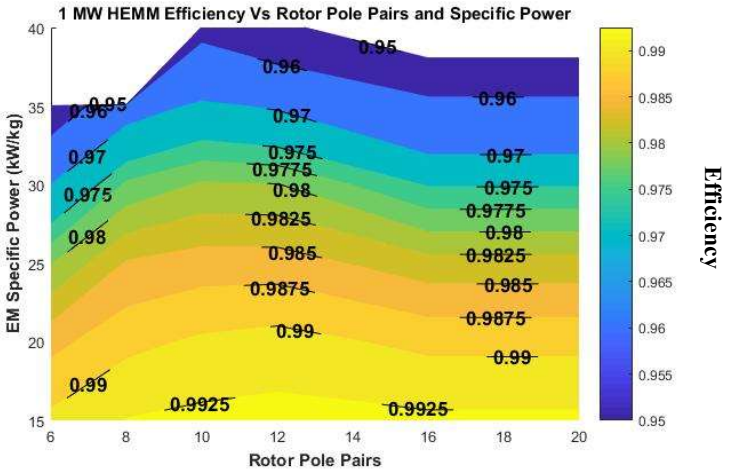

Figure 10 Geared HEMM Design Tool Results at 1 MW - Efficiency versus Pole Pairs and Electromagnetic Specific Power

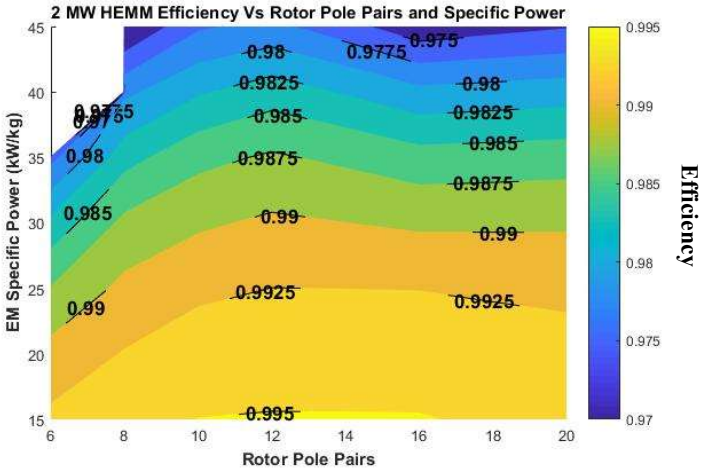

Figure 11 Geared HEMM Design Tool Results at 2 MW - Efficiency versus Pole Pairs and Electromagnetic Specific Power

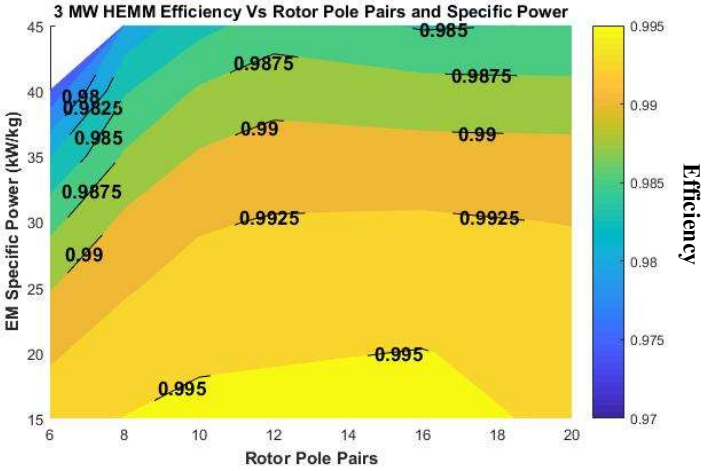

Figure 12 Geared HEMM Design Tool Results at 3 MW - Efficiency versus Pole Pairs and Electromagnetic Specific Power

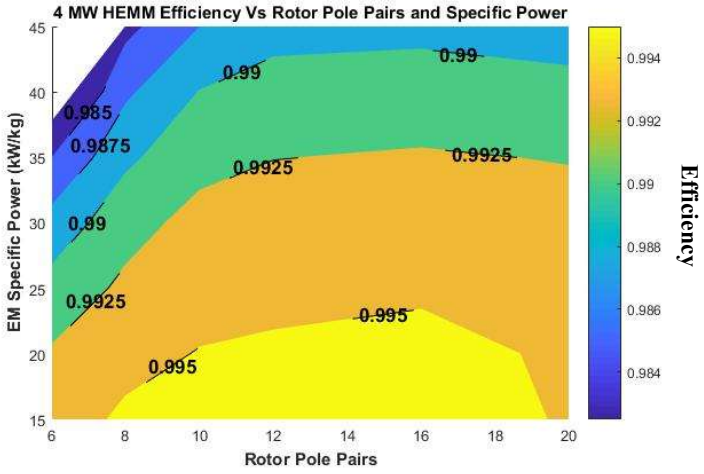

Figure 13 Geared HEMM Design Tool Results at 4 MW - Efficiency versus Pole Pairs and Electromagnetic Specific Power

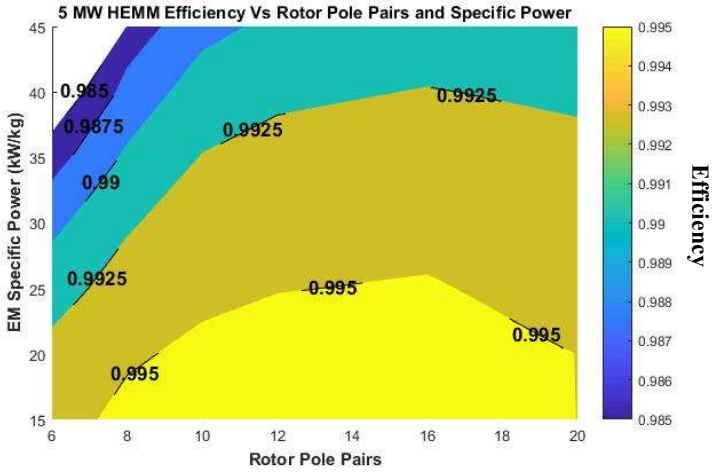

Figure 14 Geared HEMM Design Tool Results at 5 MW - Efficiency versus Pole Pairs and Electromagnetic Specific Power

In Figures 10 thru 14, the optimum RPM in most cases corresponded to the 1000 Hz electrical frequency limit applied in the design study. The optimum rotational speeds can therefore typically be calculated by

$$RPM = \frac{1000}{Rotor_{Pole_{Pairs}}} * 60 \tag{6}$$

and range from 10,000 RPM at 6 Pole Pairs to 3,000 RPM at 20 Pole Pairs. The only exceptions to this correlation are high power, low specific power designs for which lower rotational speeds were optimum due to long stack lengths and lower resistive losses (see Appendix C).

In general, the design tool favored lower RPM designs than expected. Especially at the higher power levels where optimum RPM is predicted to be in the range of 3500 RPM (Figures 13 and 14). The cause of this trend is rotor radius effects. Figure 15 shows how rotor radius trends with pole count and RPM in the design tool results.

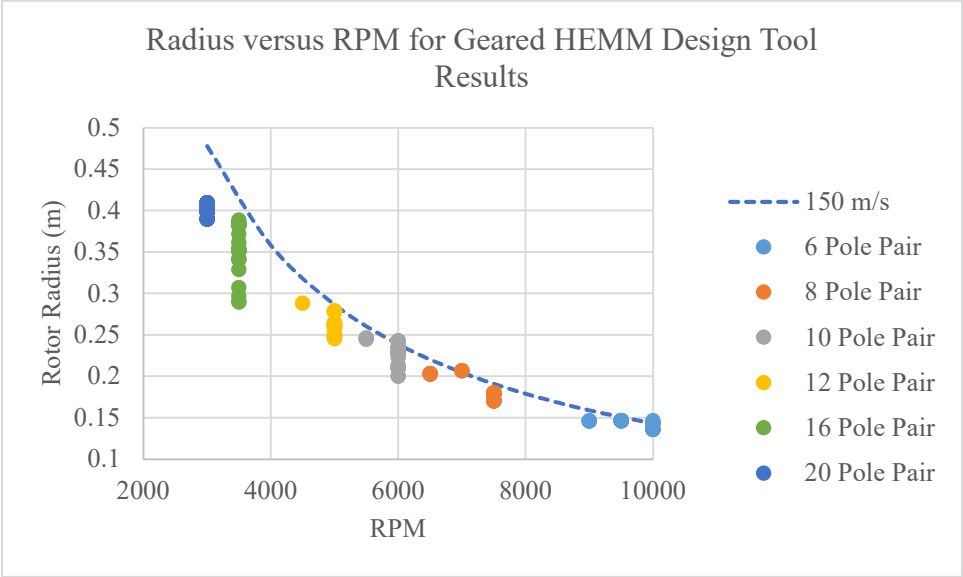

Figure 15 Rotor Radius versus RPM for Geared HEMM Design Tool Results

In the geared design studies, rotor radius was only limited at a given RPM by the centripetal loading on the coil. The maximum optimum tip speed in Figure 15 (about 150 m/s) did not result from a constraint on tip speed but because

the mass of each superconducting coil per meter of motor stack length increased approximately linearly with increased radius. Figure 16 shows the trend between coil mass and radius.

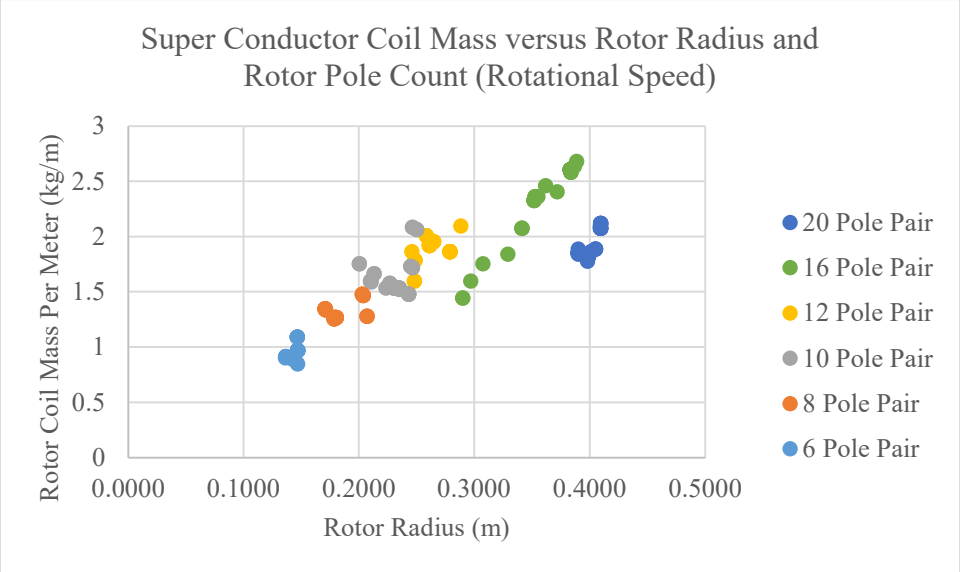

Figure 16 Superconducting coil mass per meter of motor stack length versus rotor radius and pole count for geared design tool results

The mass of the coil per meter of motor stack length increased linearly with RPM at lower pole counts, because at the assumed operating temperature of the rotor coils, the design tool found that more superconducting turns were more valuable for machine efficiency than more rotor iron. Correspondingly, the rotor iron tooth width stayed roughly constant and at its minimum value throughout the solution space (see tables in Appendix C). With both radius and coil mass increasing with reduced RPM at a constant tip speed, rotor coil centripetal loading stays constant, as shown in Figure 17. The trend does break down at high pole counts and low rpm, due to aspect ratio effects that make the 150 m/s tip speed no longer optimum. In fact, at each combination of power and specific power.

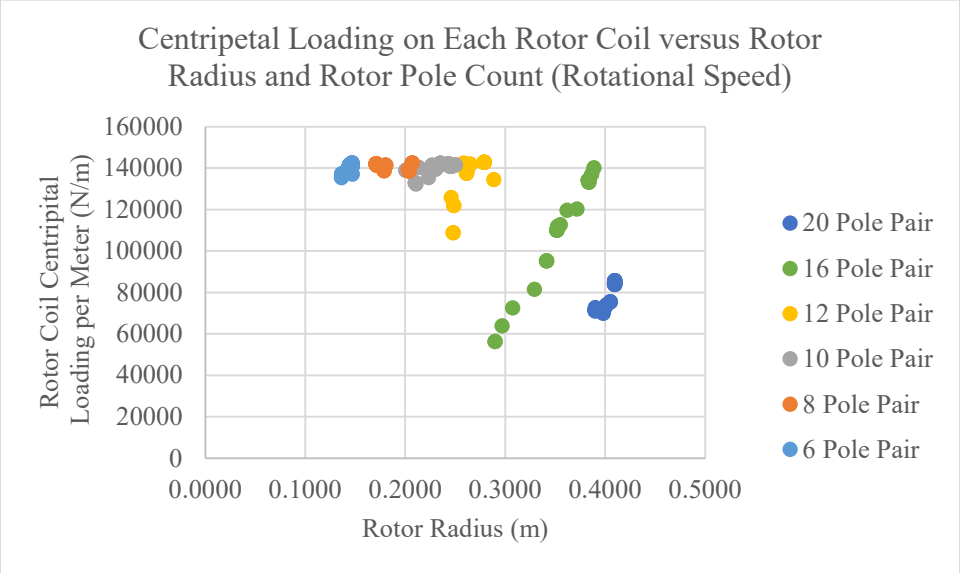

Figure 17 Superconducting coil centripetal loading per meter versus rotor radius and pole count for geared design tool results

Relatively low motor rotational speeds were found to be optimum in the design study because the centripetal loading constraint made it such that lower speeds both allowed for increased machine radius and increase superconducting turn counts on the rotor. It is however important to note that the benefits of increased superconducting turns on the rotor as speed reduces and radius increases has a significant monetary cost. Figure 18 shows the total cost of superconductor versus pole count, which is inversely proportional to rotational speed, for the 3 MW design tool results. Figure 19 shows the relationship between superconductor cost and machine efficiency for all the geared HEMM design tool results. If a cost constraint had been included in the design optimization, like was done in the redesign of HEMM [15], it is possible that higher rpm would be more optimum as Figure 19 suggests; however, the results in this paper cannot confirm that, and more studies would need to be completed.

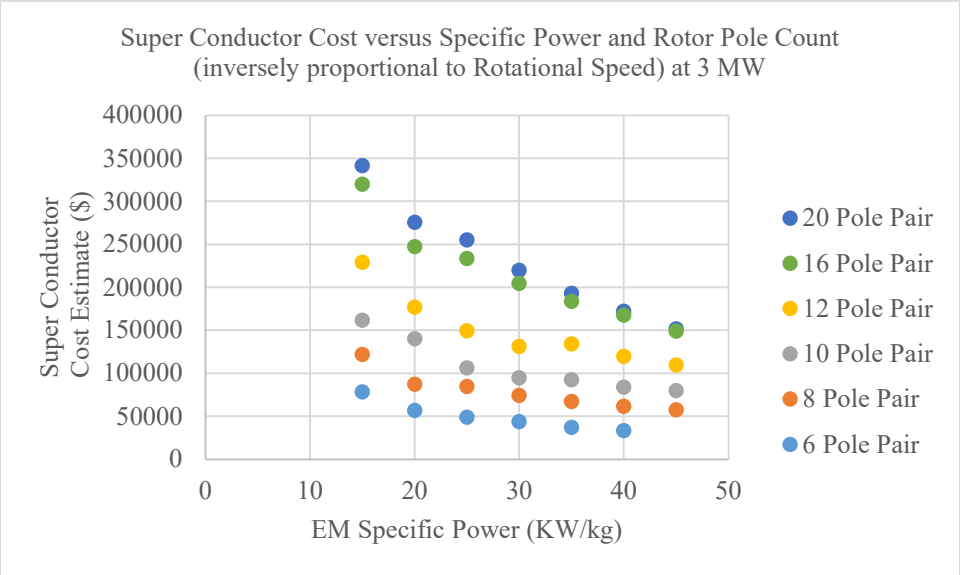

Figure 18 Superconductor Cost Estimate for 3 MW Geared HEMM Design Tool Results, assuming $60 per meter of superconductor.

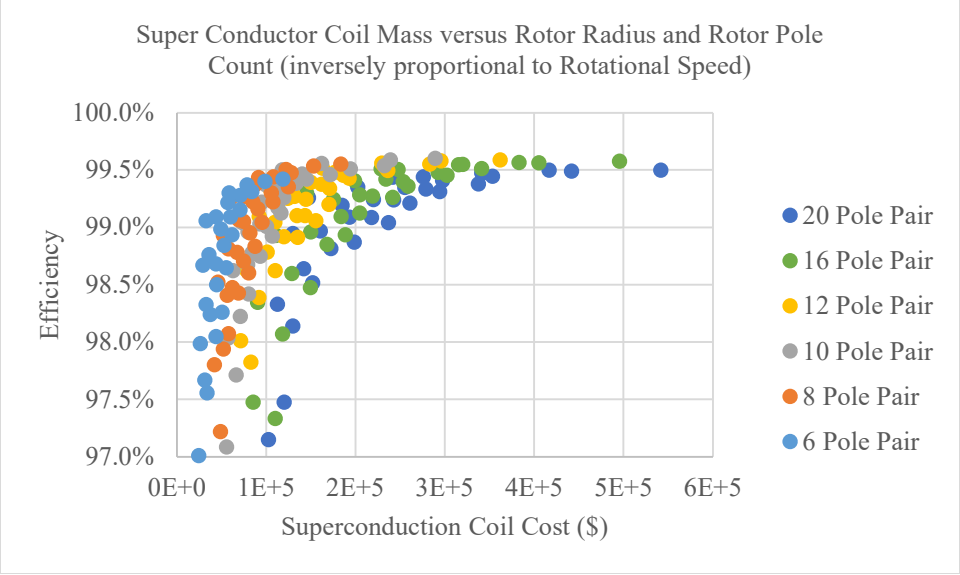

Figure 19 Machine Efficiency versus Superconductor Cost for All Geared HEMM Design tool Results, assuming $60 per meter of superconductor.

In general, the low optimum RPM results of the geared design studies make it unlikely that a geared version of the HEMM technology would be optimum in an electric aircraft's drivetrain unless propeller RPM were very low (less

than 1500 RPM). However, this paper only attempts to quantify optimum electromagnetic machine performance with HEMM technology and does not try to estimate total driveline mass and therefore cannot fully answer that question. The following section provides direct drive HEMM results with a comparison to the geared designs.

B. Direct Drive Results

For direct drive motor design, motor RPM and rotor tip speed limits are difficult to select for a general evaluation of a motor technology. For the study presented here, RPM was held fixed at 3000 RPM, a typical RPM for fixed wing aircraft propellers. Design tool runs were completed with three different rotor tip speed limits. The results of these design runs are shown in Figures 20 through 24. In each figure, the results are compared to the optimum designs from the geared studies in which RPM and tip speed were both free variables. Appendix D contains tabulated results for all the direct drive HEMM design tool results.

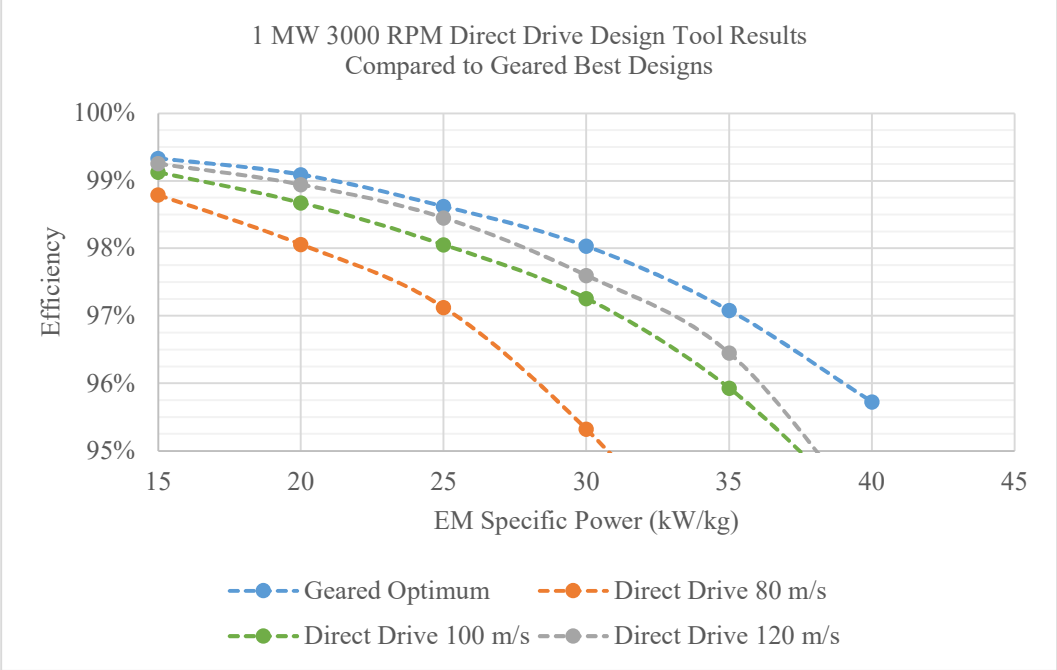

Figure 20 1 MW 3000 RPM Direct Drive Design Tool Results Compared to the Best Geared Design Tool Results at 1 MW

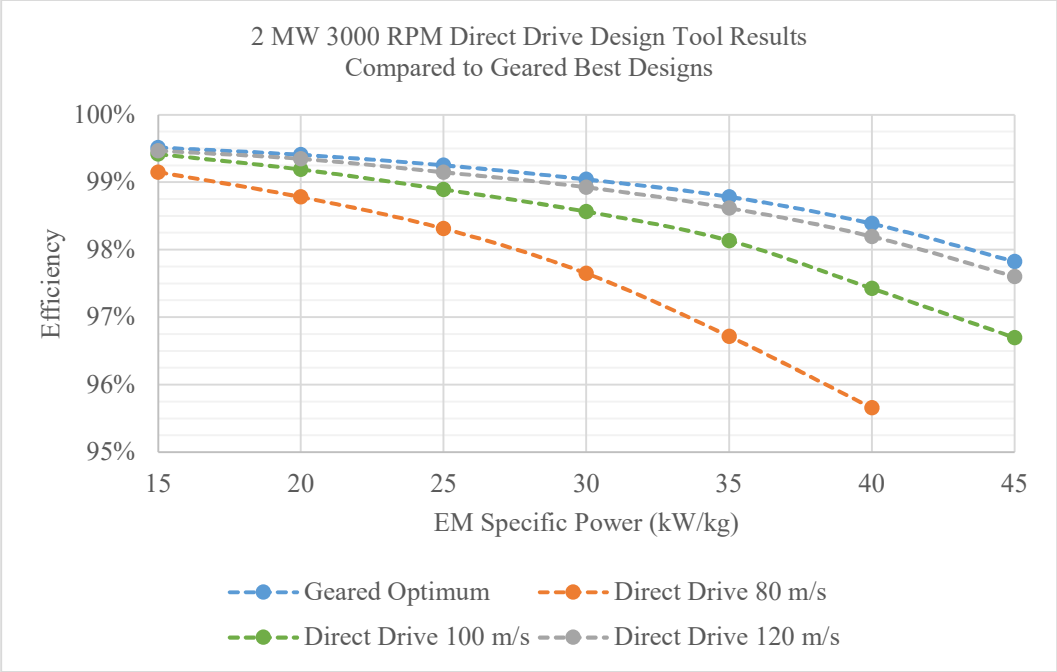

Figure 21 2 MW 3000 RPM Direct Drive Design Tool Results Compared to the Best Geared Design Tool Results at 2 MW

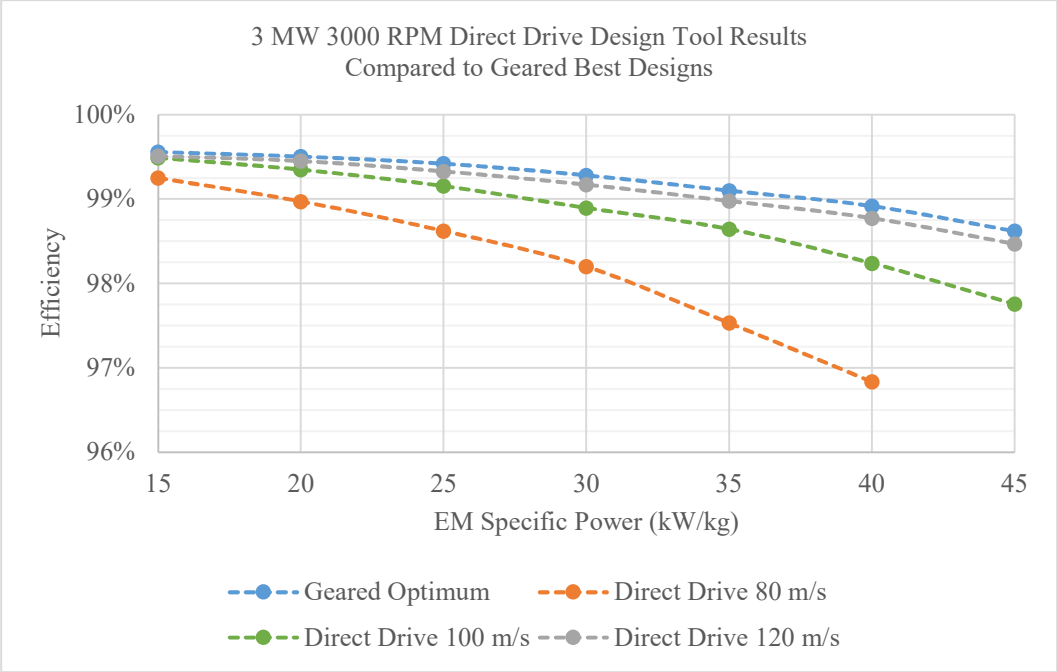

Figure 22 3 MW 3000 RPM Direct Drive Design Tool Results Compared to the Best Geared Design Tool Results at 3 MW

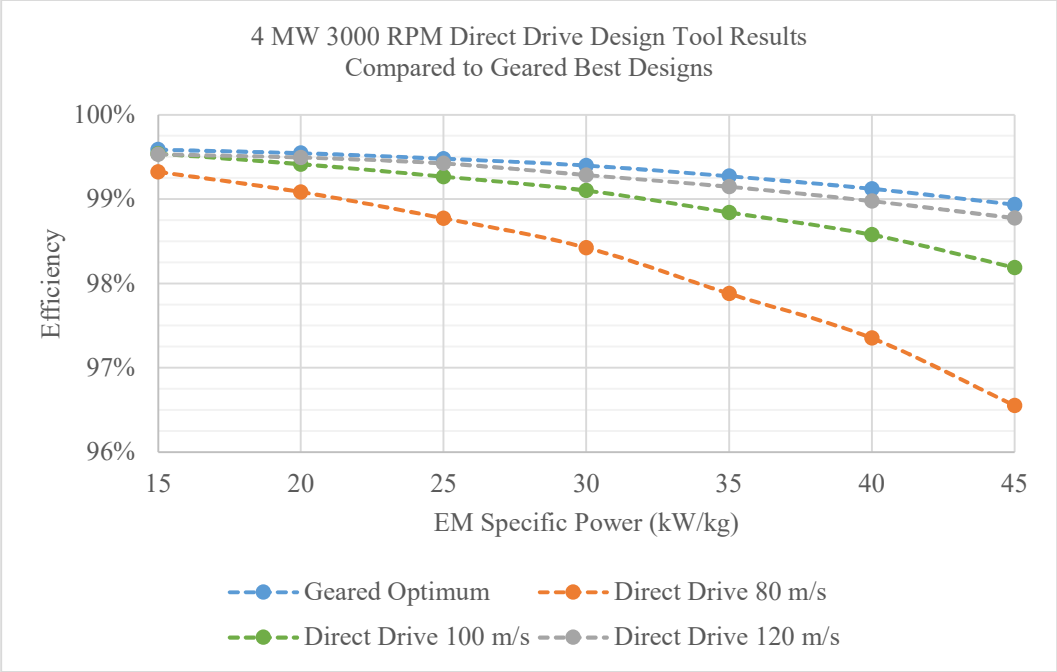

Figure 23 4 MW 3000 RPM Direct Drive Design Tool Results Compared to the Best Geared Design Tool Results at 4 MW

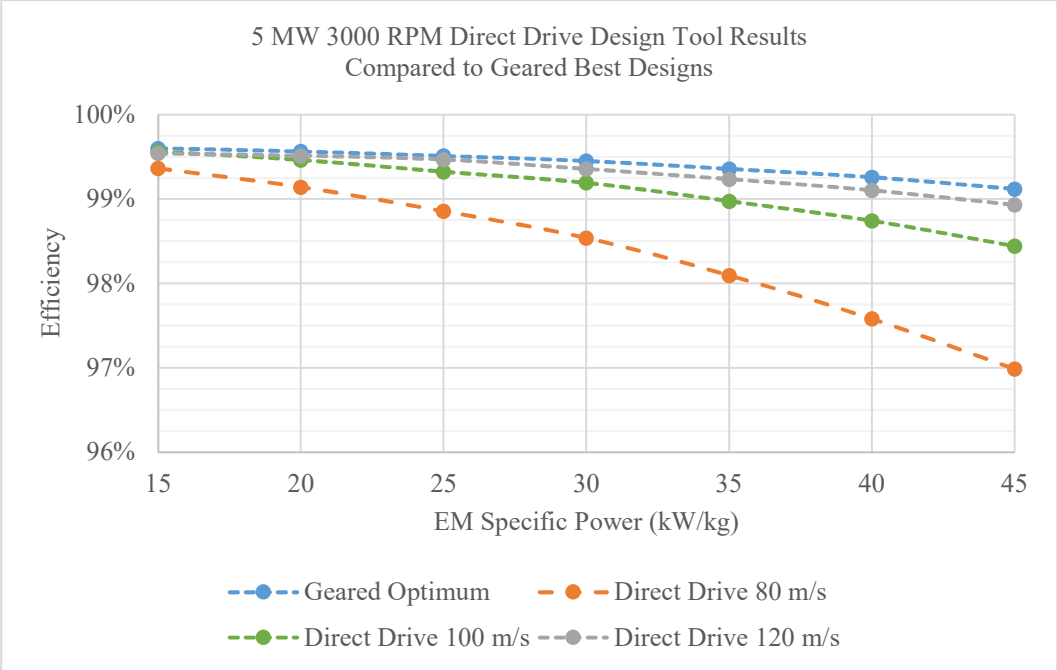

Figure 24 5 MW 3000 RPM Direct Drive Design Tool Results Compared to the Best Geared Design Tool Results at 5 MW

In Figures 20 through 24, very little performance difference exists between the geared optimum and 120 m/s tip speed direct drive case. This is a result of the centripetal loading constraint and aspect ratio effects discussed in Section IV-A, which led to the geared designs having relatively low optimum rotational speeds and rotor tip speeds. This small difference between the achievable performance of geared and 120 m/s tip speed direct drive HEMM motors suggests

that, as long as sufficient tip speed can be maintained in a direct drive HEMM, a geared drive will perform substantially worse than a direct drive system when gearbox losses and mass are included.

When tip speed is constrained to lower values, as it would be in real direct drive propulsor design for fan mass, efficiency, and noise considerations, it becomes more likely that a geared drive would be the better choice. The electromagnetic specific power at which 99% efficiency is achievable is doubled at all power levels comparing the geared optimum results to the 80 m/s results. It is important to note that this is only the electromagnetic specific power and whether a gearbox with its efficiency and mass penalty could be justified even in this case is unclear.

The machine's radius (and thus the rotor's tip speed at a set RPM) again has compounding effects on performance. A reduction in radius both reduces the amount of superconductor on the rotor and puts the machine at a mechanical disadvantage. In the direct drive results, the designs at lower tip speeds do attempt to compensate for the lower available area for superconductor by reducing the rotor's pole count (see tables in Appendix D). This reduction in pole count with reduced tip speed corresponds to the rotor iron tooth width staying close to its minimum value and the machine again prioritizing more superconductor in the rotor coils for maximizing efficiency. However, the reduced pole count is not fully able to maintain the total number of superconducting wires on the rotor as rotor tip speed is reduced. A comparison of the total cost of superconductor at 3 MW is shown in Figure 25 to illustrate this reduction in superconducting wire with reduced tip speed.

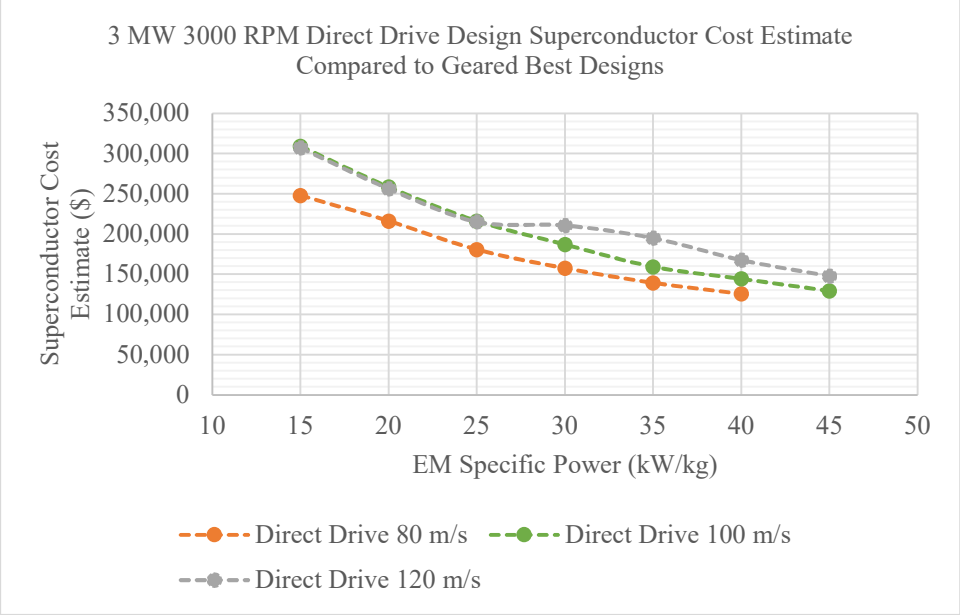

Figure 25 Superconductor Cost Comparison between Geared and Direct Drive HEMM Design tool Results at 3 MW, assuming $60 per meter of superconductor.

Comparing the superconductor cost curves in Figure 25 to the corresponding machine performance data in Figure 22, some correlation can be observed. Both the more significant drop in performance going from 100 m/s to 80 m/s than from 120 m/s to 100 m/s and the increasing difference in achievable efficiency between 100 m/s and 120 m/s with increased specific power can be somewhat correlated with the trends in cost.

V. Conclusion

In this paper, the achievable electromagnetic performance of the HEMM technology was evaluated across a wide design space. A design tool was developed that implemented a novel approach for evaluating the performance of partially superconducting machines across a design space with minimal computational cost. The approach was used to study the effects of rotation speed, pole count, power, tip speed, and specific power on the machine's efficiency. Within the constraints of the current NASA HEMM technology, it was found that a direct drive system is likely to provide optimum performance unless rotor tip speed is constrained to a small value due to fan considerations. The importance of the quantity (and thus cost) of superconductor for achieving optimal performance was also shown. Future work in this area targets further development of the HEMM design tool to include other components in the drivetrain like the motor's inverter, the cryocooler, and the propulsion fan. Additional work targets the exploration of trades on superconductor temperature, superconductor cost, and other machine topologies.

Appendix

A. Electromagnetic Loss Models

At each rotor current and stator current value evaluated using the FEA model, spatial magnetic field data is exported from the model for both the stator windings and the stator iron. This is done at 5 arc segments with a 0.5 mm circumferential resolution in both the iron and the stator windings. The spatial field data from each arc segment is then used as an approximation of the time varying field in both the stator windings and iron. This approximation should be fairly accurate for any good machine design since the rotor magnetic field will dominate the magnetic field in the stator region and because there is no spatial variation of permeability in the stator to change the shape of the field the rotor produces as it rotates.

The stator iron field data is turned into an iron loss per meter stack length value using the improved generalized Steinmetz equation [18]. For each arc segment this is implemented as

$$Pperm_{iron} = k1 * \rho_{iron} * 2\pi R * t_{layer} * \left(B_{pk-pk}\right)^{\beta-\alpha} * \frac{1}{N}\sum_{n=1}^{N}\left(\frac{B_{n+1} - B_n}{\Delta t}\right)^{\alpha} \tag{7}$$

where $Pperm_{iron}$ is stator iron loss per meter stack length, $k1$, α, and β are loss coefficients, R is the radius of a given arc segment magnetic field was extracted from, t_{layer} is the radial thickness the of the area around the arc segment the B field data is assumed to be accurate for, B_{pk-pk} is the peak to peak flux density of the magnetic field data, B_n is magnetic field at the nth point along the arc segment, and Δt is the time step equivalent to the spatial increments between data points along the arc segment. Δt is calculated as

$$\Delta t = \frac{1}{N} * \frac{1}{f_{elec}} \tag{8}$$

The stator winding field data for each arc segment is similarly turned into a proximity loss coefficient

$$C_{proximity} = \frac{1}{12} 2\pi R * t_{layer} * \frac{1}{N}\sum_{n=1}^{N}\left(\frac{B_{n+1} - B_n}{\Delta t}\right)^2 \tag{9}$$

where $C_{proximity}$ is the loss coefficient. $C_{proximity}$ is defined such that

$$P_{proximity} = F_{Slot} * C_{proximity} * d_{wire}^2 * Stack * \sigma_{copper} \tag{10}$$

where F_{Slot} is the winding slot fill d_{wire} is the stator litz wire strand diameter, Stack is the stator stack length, and σ_{copper} is the conductivity of copper.

Iron loss and proximity loss coefficients at each arc segment are summed for each combination of stator current and rotor current the FEA simulation is solved for. Scattered interpolant functions are then produced for the iron and proximity loss coefficients as a function of both rotor and stator current.

B. Winding Analysis

Winding analysis of the machine slots is carried out to optimize the winding turn count, strand count, and wire gauge to minimize the combined total of winding proximity losses and winding resistive losses. Possible turn counts per slot are predicted for each geometry based on the bus voltage and the required slot current. Basic geometric relationship for packing circles into rectangles efficiently are used to determine the size of the turns for each possible turn count and then the number of wires of each possible gauge count that can fit in that turn size. A packing factor is included to keep copper fill percentage for the winding in the 28-40% range, corresponding to the copper fill in HEMM's windings. Winding insulation thicknesses are accounted for by taking the thickness of the Nomex away from the turn radii and using the NEMA 1000 standard definition of MW-16 insulated wire sizes [19].

Proximity losses are predicted for each case using equation 10 in Appendix A.

DC resistivity of the copper windings is calculated at the winding temperature. The winding temperature is assumed to be 150˚C for the first winding analysis iteration and then on the second iteration takes the predicted peak winding temperature from the model described in Section III-D. AC resistivity is estimated in each case for the litz wire bundles as

$$R_{AC} = R_{DC} * \frac{(1 + \pi * N_{strands})^2 * d_{wire}^6}{192 * \delta^4 W_{slot}^2} \tag{11}$$

where R_{AC} is the winding AC resistivity, R_{DC} is the DC resistivity, $N_{strands}$ is the total number of strands in a slot, d_{wire} is the bare wire strand diameter, δ is skin depth, and W_{slot} is the slot width.

Total losses (proximity, AC resistive, and Iron) are summed up for each case of rotor current, required stator current, turn counts, and wire gauge and the optimum case is selected. The winding transverse thermal conductivity is then predicted using

$$k_{w2} = \frac{k_{epoxy}\left((1+F_{slot})k_{copper} + (1-F_{Slot}) * k_{epoxy}\right)}{(1-F_{Slot}) * k_{Copper} + (1+F_{Slot}) * k_{epoxy}}. \quad (12)$$

All losses and the winding transverse thermal conductivity are fed to the Thermal model of Section III-D.

C. Geared HEMM Data

Table 4 1 MW Geared HEMM Results

Rotor Back Iron Thickness Ratio	Rotor Iron Tooth Width (m)	Stator Back Iron Thickness (m)	Stator Winding Radial Thickness (m)	Rotor Pole Pair Count	Rotor Radius (m)	Specific Power (kW/kg)	RPM	Stack Length (m)	Winding Resistive Loss (W)	Winding Eddy Current Loss (W)	Stator Iron Losses (W)	Efficiency
0.4794	0.0474	0.0188	0.0086	6	0.144	15	10000	0.131	7116	199	2188	99.06%
0.5273	0.0431	0.0160	0.0087	6	0.137	20	10000	0.108	11447	373	1674	98.67%
0.5273	0.0431	0.0160	0.0087	6	0.137	25	10000	0.084	18837	436	1301	97.98%
0.5273	0.0431	0.0160	0.0087	6	0.137	30	10000	0.068	28951	840	1047	97.01%
0.4730	0.0431	0.0180	0.0061	6	0.136	35	10000	0.060	47050	675	942	95.36%
0.4700	0.0362	0.0145	0.0131	8	0.171	15	7500	0.147	5043	237	2195	99.26%
0.4960	0.0358	0.0151	0.0099	8	0.171	20	7500	0.110	8748	207	1882	98.93%
0.4960	0.0358	0.0151	0.0099	8	0.171	25	7500	0.084	12935	638	1432	98.52%
0.4960	0.0358	0.0151	0.0099	8	0.171	30	7500	0.067	20871	479	1140	97.80%
0.4960	0.0358	0.0151	0.0099	8	0.171	35	7500	0.054	31849	921	927	96.74%
0.4700	0.0403	0.0182	0.0131	10	0.231	15	6000	0.107	4370	300	2247	99.31%
0.4737	0.0333	0.0159	0.0097	10	0.213	20	6000	0.097	7425	265	2000	99.04%
0.4786	0.0331	0.0160	0.0090	10	0.210	25	6000	0.076	11910	527	1525	98.62%
0.4786	0.0331	0.0160	0.0090	10	0.210	30	6000	0.060	18244	622	1196	98.03%
0.4700	0.0281	0.0172	0.0060	10	0.201	35	6000	0.058	28481	536	1031	97.08%
0.4700	0.0281	0.0172	0.0060	10	0.201	40	6000	0.048	42744	1038	854	95.73%
0.4600	0.0324	0.0169	0.0144	12	0.262	15	5000	0.104	4172	337	2176	99.34%
0.4735	0.0315	0.0175	0.0098	12	0.261	20	5000	0.080	6851	320	1963	99.09%
0.4905	0.0309	0.0180	0.0070	12	0.249	25	5000	0.070	12143	241	1570	98.62%
0.4952	0.0292	0.0170	0.0079	12	0.246	30	5000	0.055	18367	734	1188	98.01%
0.5125	0.0331	0.0176	0.0070	12	0.248	35	5000	0.044	29988	539	1009	96.94%
0.5125	0.0331	0.0176	0.0070	12	0.248	40	5000	0.036	48919	1008	815	95.17%
0.5149	0.0294	0.0228	0.0099	16	0.362	15	3500	0.077	4555	478	2026	99.30%
0.4600	0.0311	0.0195	0.0076	16	0.329	20	3500	0.075	8760	312	1745	98.93%
0.5107	0.0280	0.0150	0.0070	16	0.297	25	3500	0.075	14730	558	1521	98.35%
0.5097	0.0280	0.0161	0.0069	16	0.307	30	3500	0.052	24099	670	1127	97.48%
0.5255	0.0285	0.0143	0.0060	16	0.290	35	3500	0.052	37643	482	1040	96.23%
0.5255	0.0285	0.0143	0.0060	16	0.290	40	3500	0.042	59636	908	844	94.22%
0.4939	0.0304	0.0160	0.0126	20	0.405	15	3000	0.084	4745	396	2343	99.26%
0.4671	0.0283	0.0160	0.0078	20	0.390	20	3000	0.072	8076	371	2204	98.95%
0.4671	0.0283	0.0160	0.0078	20	0.390	25	3000	0.051	14776	675	1553	98.33%
0.4737	0.0280	0.0160	0.0074	20	0.390	30	3000	0.037	27482	732	1136	97.15%
0.4756	0.0284	0.0159	0.0064	20	0.390	35	3000	0.029	52592	1238	908	94.81%

Table 5 2 MW Geared HEMM Results

Rotor Back Iron Thickness Ratio	Rotor Iron Tooth Width (m)	Stator Back Iron Thickness (m)	Stator Winding Radial Thickness (m)	Rotor Pole Pair Count	Rotor Radius (m)	Specific Power (kW/kg)	RPM	Stack Length (m)	Winding Resistive Loss (W)	Winding Eddy Current Loss (W)	Stator Iron Losses (W)	Efficiency
0.4874	0.0461	0.0184	0.0099	6	0.147	15	9000	0.267	9621	384	4111	99.30%
0.4893	0.0478	0.0182	0.0093	6	0.147	20	9500	0.197	14283	770	3295	99.09%
0.4794	0.0474	0.0188	0.0086	6	0.144	25	10000	0.159	21458	969	2650	98.76%
0.4901	0.0464	0.0182	0.0085	6	0.142	30	10000	0.135	31068	761	2208	98.33%
0.5273	0.0431	0.0160	0.0087	6	0.137	35	10000	0.126	44330	1536	1922	97.67%
0.4961	0.0470	0.0165	0.0180	8	0.204	15	6500	0.211	7462	337	3580	99.43%
0.5256	0.0407	0.0144	0.0130	8	0.180	20	7500	0.207	10704	367	3760	99.26%
0.4837	0.0360	0.0138	0.0131	8	0.171	25	7500	0.183	15260	760	2834	99.07%
0.5025	0.0403	0.0168	0.0095	8	0.180	30	7500	0.135	20741	728	2598	98.81%
0.4960	0.0358	0.0151	0.0099	8	0.171	35	7500	0.128	29250	927	2190	98.41%
0.4736	0.0386	0.0191	0.0192	10	0.227	15	6000	0.223	6563	405	3034	99.50%
0.5117	0.0419	0.0194	0.0102	10	0.235	20	6000	0.170	7892	586	4218	99.37%
0.4729	0.0394	0.0150	0.0142	10	0.229	25	6000	0.140	12581	351	3136	99.20%
0.4700	0.0404	0.0154	0.0131	10	0.230	30	6000	0.112	17586	779	2649	98.96%
0.4737	0.0333	0.0159	0.0097	10	0.213	35	6000	0.114	23702	783	2362	98.68%
0.4740	0.0335	0.0162	0.0089	10	0.211	40	6000	0.100	33160	1016	2026	98.22%
0.4786	0.0331	0.0160	0.0090	10	0.210	45	6000	0.087	44264	821	1740	97.71%
0.4600	0.0324	0.0169	0.0200	12	0.261	15	5000	0.224	5908	485	3368	99.51%
0.4938	0.0378	0.0155	0.0161	12	0.279	20	5000	0.151	7624	516	3967	99.40%
0.4600	0.0320	0.0178	0.0106	12	0.262	25	5000	0.141	11177	548	3345	99.25%
0.4710	0.0322	0.0174	0.0100	12	0.261	30	5000	0.115	16036	445	2860	99.04%
0.4659	0.0306	0.0163	0.0106	12	0.258	35	5000	0.097	21317	927	2360	98.78%
0.4731	0.0322	0.0175	0.0093	12	0.261	40	5000	0.081	29533	1230	2019	98.39%
0.4905	0.0309	0.0180	0.0070	12	0.249	45	5000	0.081	41647	1033	1797	97.82%
0.4794	0.0289	0.0258	0.0115	16	0.353	15	3500	0.187	5157	994	3701	99.51%
0.5164	0.0320	0.0255	0.0081	16	0.384	20	3500	0.121	7212	916	3794	99.41%
0.4600	0.0317	0.0236	0.0081	16	0.383	25	3500	0.094	11386	694	3162	99.24%
0.5144	0.0320	0.0232	0.0076	16	0.372	30	3500	0.079	18058	511	2462	98.96%
0.4600	0.0304	0.0191	0.0077	16	0.341	35	3500	0.083	25216	1016	2227	98.60%
0.4600	0.0304	0.0191	0.0077	16	0.341	40	3500	0.068	36318	1254	1832	98.07%
0.4600	0.0304	0.0191	0.0077	16	0.341	45	3500	0.057	52277	985	1535	97.33%
0.4726	0.0303	0.0160	0.0140	20	0.399	15	3000	0.212	5470	827	5025	99.44%
0.4692	0.0299	0.0158	0.0116	20	0.401	20	3000	0.156	7905	744	4422	99.35%
0.4874	0.0280	0.0160	0.0101	20	0.410	25	3000	0.113	11890	672	3763	99.19%
0.4909	0.0285	0.0160	0.0099	20	0.409	30	3000	0.088	17382	509	2962	98.97%
0.4671	0.0283	0.0160	0.0078	20	0.390	35	3000	0.087	23796	1153	2675	98.64%
0.4671	0.0283	0.0160	0.0078	20	0.390	40	3000	0.072	34318	1430	2197	98.14%
0.4671	0.0283	0.0160	0.0078	20	0.390	45	3000	0.060	48826	1134	1837	97.48%

Table 6 3 MW Geared HEMM Results

Rotor Back Iron Thickness Ratio	Rotor Iron Tooth Width (m)	Stator Back Iron Thickness (m)	Stator Winding Radial Thickness (m)	Rotor Pole Pair Count	Rotor Radius (m)	Specific Power (kW/kg)	RPM	Stack Length (m)	Winding Resistive Loss (W)	Winding Eddy Current Loss (W)	Stator Iron Losses (W)	Efficiency
0.4874	0.0461	0.0184	0.0099	6	0.147	15	9000	0.407	12195	589	6276	99.37%
0.4893	0.0478	0.0182	0.0093	6	0.147	20	9500	0.301	18169	443	5053	99.22%
0.4893	0.0478	0.0182	0.0093	6	0.147	25	9500	0.239	25826	910	3996	98.99%
0.4893	0.0478	0.0182	0.0093	6	0.147	30	9500	0.197	35724	1126	3274	98.68%
0.4794	0.0474	0.0188	0.0086	6	0.144	35	10000	0.171	49974	948	2836	98.24%
0.4778	0.0495	0.0178	0.0079	6	0.147	40	10000	0.148	70609	1937	2644	97.56%
0.4961	0.0470	0.0165	0.0180	8	0.204	15	6500	0.331	8799	530	5617	99.50%
0.4911	0.0509	0.0122	0.0231	8	0.207	20	7000	0.234	13982	756	4195	99.37%
0.4920	0.0401	0.0148	0.0118	8	0.179	25	7500	0.263	18264	476	4821	99.22%
0.4920	0.0401	0.0148	0.0118	8	0.179	30	7500	0.215	23741	1009	3933	99.05%
0.5025	0.0403	0.0168	0.0095	8	0.180	35	7500	0.179	32164	1475	3421	98.78%
0.5025	0.0403	0.0168	0.0095	8	0.180	40	7500	0.154	42364	1214	2951	98.47%
0.5023	0.0402	0.0168	0.0094	8	0.180	45	7500	0.135	55395	1006	2585	98.07%
0.4736	0.0386	0.0191	0.0192	10	0.227	15	6000	0.350	7909	640	4772	99.56%
0.4957	0.0423	0.0196	0.0134	10	0.245	20	5500	0.240	10066	731	5317	99.47%
0.5040	0.0450	0.0201	0.0119	10	0.243	25	6000	0.190	14169	627	4742	99.35%
0.5040	0.0450	0.0201	0.0119	10	0.243	30	6000	0.154	19254	496	3852	99.22%
0.4700	0.0404	0.0154	0.0131	10	0.230	35	6000	0.152	24781	1042	3597	99.03%
0.5117	0.0418	0.0194	0.0102	10	0.235	40	6000	0.122	32472	1597	3014	98.78%
0.5161	0.0381	0.0174	0.0097	10	0.223	45	6000	0.121	44150	1342	2761	98.42%
0.4600	0.0324	0.0169	0.0200	12	0.261	15	5000	0.356	7158	773	5354	99.56%
0.4938	0.0378	0.0155	0.0161	12	0.279	20	5000	0.246	8328	841	6435	99.48%
0.4938	0.0378	0.0155	0.0161	12	0.279	25	5000	0.189	12791	636	4958	99.39%
0.4938	0.0378	0.0155	0.0161	12	0.279	30	5000	0.151	17565	497	3973	99.27%
0.4659	0.0306	0.0163	0.0106	12	0.258	35	5000	0.161	22711	586	3912	99.10%
0.4728	0.0322	0.0172	0.0100	12	0.263	40	5000	0.132	28128	1319	3357	98.92%
0.4731	0.0322	0.0175	0.0093	12	0.261	45	5000	0.117	37252	1775	2927	98.62%
0.4794	0.0289	0.0258	0.0115	16	0.353	15	3500	0.299	6143	1587	5900	99.55%
0.4794	0.0291	0.0257	0.0120	16	0.352	20	3500	0.215	9740	1082	4099	99.51%
0.4600	0.0317	0.0236	0.0081	16	0.383	25	3500	0.159	10950	1182	5335	99.42%
0.4600	0.0317	0.0236	0.0081	16	0.383	30	3500	0.126	16489	925	4251	99.28%
0.4600	0.0317	0.0236	0.0081	16	0.383	35	3500	0.103	23219	738	3476	99.09%
0.4600	0.0317	0.0236	0.0081	16	0.383	40	3500	0.086	30445	1579	2874	98.85%
0.4834	0.0293	0.0206	0.0078	16	0.355	45	3500	0.090	41953	1970	2594	98.47%
0.4726	0.0303	0.0160	0.0140	20	0.399	15	3000	0.339	7829	1088	7061	99.47%
0.4939	0.0304	0.0160	0.0126	20	0.405	20	3000	0.241	9052	1135	6708	99.44%
0.4874	0.0280	0.0160	0.0101	20	0.410	25	3000	0.189	12286	1137	6310	99.35%
0.4874	0.0280	0.0160	0.0101	20	0.410	30	3000	0.151	16989	894	5038	99.24%
0.4921	0.0285	0.0160	0.0100	20	0.410	35	3000	0.125	22711	716	4171	99.09%
0.4671	0.0283	0.0160	0.0078	20	0.390	40	3000	0.125	30483	1651	3844	98.81%
0.4859	0.0307	0.0154	0.0091	20	0.398	45	3000	0.100	39956	1995	3220	98.52%

Table 7 4 MW Geared HEMM Results

Rotor Back Iron Thickness Ratio	Rotor Iron Tooth Width (m)	Stator Back Iron Thickness (m)	Stator Winding Radial Thickness (m)	Rotor Pole Pair Count	Rotor Radius (m)	Specific Power (kW/kg)	RPM	Stack Length (m)	Winding Resistive Loss (W)	Winding Eddy Current Loss (W)	Stator Iron Losses (W)	Efficiency
0.4874	0.0461	0.0184	0.0099	6	0.147	15	9000	0.548	14857	793	8441	99.40%
0.4893	0.0478	0.0182	0.0093	6	0.147	20	9500	0.406	21699	599	6811	99.28%
0.4893	0.0478	0.0182	0.0093	6	0.147	25	9500	0.322	30017	1237	5401	99.09%
0.4893	0.0478	0.0182	0.0093	6	0.147	30	9500	0.267	40826	1541	4439	98.84%
0.4794	0.0474	0.0188	0.0086	6	0.144	35	10000	0.233	55849	1304	3848	98.50%
0.4893	0.0478	0.0182	0.0093	6	0.147	40	9500	0.197	73799	2608	3276	98.05%
0.4961	0.0470	0.0165	0.0180	8	0.204	15	6500	0.451	10341	723	7653	99.53%
0.4911	0.0509	0.0122	0.0231	8	0.207	20	7000	0.324	16364	391	5807	99.44%
0.5251	0.0466	0.0157	0.0168	8	0.203	25	6500	0.265	22095	1174	4926	99.30%
0.5256	0.0407	0.0144	0.0130	8	0.180	30	7500	0.283	27382	1293	5163	99.16%
0.5025	0.0403	0.0168	0.0095	8	0.180	35	7500	0.244	36447	1299	4701	98.95%
0.4920	0.0401	0.0148	0.0118	8	0.179	40	7500	0.215	46975	1491	3945	98.71%
0.5025	0.0403	0.0168	0.0095	8	0.180	45	7500	0.186	58936	1413	3561	98.43%
0.5210	0.0382	0.0210	0.0190	10	0.246	15	5000	0.407	9466	917	6231	99.59%
0.5210	0.0395	0.0209	0.0142	10	0.250	20	5000	0.308	12666	926	6135	99.51%
0.5035	0.0429	0.0190	0.0143	10	0.247	25	5500	0.253	16918	734	5708	99.42%
0.5040	0.0450	0.0201	0.0119	10	0.243	30	6000	0.214	21098	692	5339	99.33%
0.4700	0.0404	0.0154	0.0131	10	0.230	35	6000	0.212	26880	1469	5017	99.17%
0.5117	0.0418	0.0194	0.0102	10	0.235	40	6000	0.170	34499	1431	4207	99.01%
0.5117	0.0418	0.0194	0.0102	10	0.235	45	6000	0.148	45221	1876	3659	98.75%
0.4600	0.0324	0.0169	0.0200	12	0.261	15	5000	0.488	8457	1074	7402	99.58%
0.4600	0.0324	0.0175	0.0187	12	0.263	20	5000	0.355	12408	866	5763	99.53%
0.4938	0.0378	0.0155	0.0161	12	0.279	25	5000	0.265	14133	893	6934	99.45%
0.4938	0.0378	0.0155	0.0161	12	0.279	30	5000	0.214	18754	709	5621	99.38%
0.4938	0.0378	0.0155	0.0161	12	0.279	35	5000	0.178	25180	574	4685	99.24%
0.4990	0.0330	0.0160	0.0121	12	0.265	40	5000	0.178	29974	1687	4544	99.10%
0.4728	0.0322	0.0172	0.0100	12	0.263	45	5000	0.162	38339	1586	4119	98.91%
0.4794	0.0291	0.0257	0.0120	16	0.352	15	3500	0.409	8809	1721	6999	99.56%
0.4794	0.0291	0.0257	0.0120	16	0.352	20	3500	0.298	11106	1506	5693	99.54%
0.4600	0.0317	0.0236	0.0081	16	0.383	25	3500	0.223	11758	1668	7509	99.48%
0.4600	0.0317	0.0236	0.0081	16	0.383	30	3500	0.180	16824	1328	6063	99.40%
0.5164	0.0320	0.0255	0.0081	16	0.384	35	3500	0.143	23817	1041	4491	99.27%
0.4600	0.0317	0.0236	0.0081	16	0.383	40	3500	0.126	30284	882	4225	99.12%
0.4600	0.0317	0.0236	0.0081	16	0.383	45	3500	0.108	37460	1973	3626	98.94%
0.4726	0.0303	0.0160	0.0140	20	0.399	15	3000	0.466	9339	1497	9707	99.49%
0.4726	0.0303	0.0160	0.0140	20	0.399	20	3000	0.339	11634	1314	8037	99.48%
0.4692	0.0299	0.0158	0.0116	20	0.401	25	3000	0.273	14734	1299	7758	99.41%
0.4874	0.0280	0.0160	0.0101	20	0.410	30	3000	0.215	18401	1277	7161	99.33%
0.4921	0.0285	0.0160	0.0100	20	0.410	35	3000	0.179	23663	1040	6001	99.24%
0.4921	0.0285	0.0160	0.0100	20	0.410	40	3000	0.152	30972	862	5088	99.09%
0.4921	0.0285	0.0160	0.0100	20	0.410	45	3000	0.131	39423	1931	4377	98.87%

Table 8 5 MW Geared HEMM Results

Rotor Back Iron Thickness Ratio	Rotor Iron Tooth Width (m)	Stator Back Iron Thickness (m)	Stator Winding Radial Thickness (m)	Rotor Pole Pair Count	Rotor Radius (m)	Specific Power (kW/kg)	RPM	Stack Length (m)	Winding Resistive Loss (W)	Winding Eddy Current Loss (W)	Stator Iron Losses (W)	Efficiency
0.4874	0.0461	0.0184	0.0099	6	0.147	15	9000	0.688	17551	997	10607	99.42%
0.4893	0.0478	0.0182	0.0093	6	0.147	20	9500	0.511	25296	755	8569	99.31%
0.4893	0.0478	0.0182	0.0093	6	0.147	25	9500	0.406	34390	1564	6807	99.15%
0.4893	0.0478	0.0182	0.0093	6	0.147	30	9500	0.336	46247	1954	5604	98.94%
0.4893	0.0478	0.0182	0.0093	6	0.147	35	9500	0.287	62159	1582	4772	98.65%
0.4893	0.0478	0.0182	0.0093	6	0.147	40	9500	0.249	81107	3346	4149	98.26%
0.4961	0.0470	0.0165	0.0180	8	0.204	15	6500	0.571	11960	915	9689	99.55%
0.4911	0.0509	0.0122	0.0231	8	0.207	20	7000	0.414	18455	500	7420	99.48%
0.5251	0.0466	0.0157	0.0168	8	0.203	25	6500	0.338	25643	560	6287	99.35%
0.5256	0.0407	0.0144	0.0130	8	0.180	30	7500	0.359	31070	1647	6554	99.22%
0.5256	0.0407	0.0144	0.0130	8	0.180	35	7500	0.305	40633	2145	5571	99.04%
0.4920	0.0401	0.0148	0.0118	8	0.179	40	7500	0.274	52010	1917	5026	98.83%
0.5025	0.0403	0.0168	0.0095	8	0.180	45	7500	0.237	64481	1823	4537	98.60%
0.5210	0.0382	0.0210	0.0190	10	0.246	15	5000	0.518	10845	1167	7924	99.60%
0.5210	0.0395	0.0209	0.0142	10	0.250	20	5000	0.393	14255	1182	7820	99.54%
0.5035	0.0429	0.0190	0.0143	10	0.247	25	5500	0.324	18900	941	7300	99.46%
0.5040	0.0450	0.0201	0.0119	10	0.243	30	6000	0.273	23325	888	6826	99.38%
0.5040	0.0450	0.0201	0.0119	10	0.243	35	6000	0.231	30835	730	5767	99.26%
0.5117	0.0418	0.0194	0.0102	10	0.235	40	6000	0.218	36992	1851	5400	99.12%
0.5117	0.0419	0.0194	0.0102	10	0.235	45	6000	0.191	47232	2461	4727	98.92%
0.4600	0.0324	0.0169	0.0200	12	0.261	15	5000	0.620	9897	1365	9405	99.59%
0.4600	0.0324	0.0175	0.0187	12	0.263	20	5000	0.454	14101	1108	7360	99.55%
0.5002	0.0372	0.0151	0.0181	12	0.288	25	4500	0.315	16750	936	7678	99.50%
0.4938	0.0378	0.0155	0.0161	12	0.279	30	5000	0.277	20497	921	7269	99.43%
0.4938	0.0378	0.0155	0.0161	12	0.279	35	5000	0.232	26387	754	6097	99.34%
0.4990	0.0330	0.0160	0.0121	12	0.265	40	5000	0.231	33582	820	5884	99.20%
0.4990	0.0330	0.0160	0.0121	12	0.265	45	5000	0.201	40589	1865	5143	99.06%
0.4794	0.0291	0.0257	0.0120	16	0.352	15	3500	0.520	10210	2189	8901	99.58%
0.4794	0.0291	0.0257	0.0120	16	0.352	20	3500	0.381	12622	1930	7286	99.57%
0.5154	0.0320	0.0260	0.0079	16	0.387	25	3500	0.271	13792	2085	8637	99.51%
0.4600	0.0317	0.0236	0.0081	16	0.383	30	3500	0.234	17891	1730	7875	99.45%
0.5164	0.0320	0.0255	0.0081	16	0.384	35	3500	0.187	25023	1370	5878	99.36%
0.5192	0.0318	0.0245	0.0076	16	0.389	40	3500	0.159	30558	1181	5523	99.26%
0.4600	0.0317	0.0236	0.0081	16	0.383	45	3500	0.144	38536	993	4826	99.12%
0.4726	0.0303	0.0160	0.0140	20	0.399	15	3000	0.593	10917	1907	12354	99.50%
0.4726	0.0303	0.0160	0.0140	20	0.399	20	3000	0.434	13230	1685	10296	99.50%
0.4939	0.0304	0.0160	0.0126	20	0.405	25	3000	0.335	17048	1565	9329	99.44%
0.4874	0.0280	0.0160	0.0101	20	0.410	30	3000	0.278	20316	1660	9285	99.38%
0.4909	0.0283	0.0160	0.0100	20	0.409	35	3000	0.234	25400	1375	7860	99.31%
0.4921	0.0285	0.0160	0.0100	20	0.410	40	3000	0.200	31981	1143	6689	99.21%
0.4921	0.0285	0.0160	0.0100	20	0.410	45	3000	0.173	41656	966	5802	99.04%

D. Direct Drive HEMM Data

Table 9 120 m/s Rotor Tip Speed HEMM 3000 RPM Design Tool Results

Rotor Back Iron Thickness Ratio	Rotor Iron Tooth Width (m)	Stator Back Iron Thickness (m)	Stator Winding Radial Thickness (m)	Rotor Pole Pair Count	Rotor Radius (m)	Power (W)	Specific Power (kW/kg)	Stack Length (m)	Winding Resistive Loss (W)	Winding Eddy Current Loss (W)	Stator Iron Losses (W)	Efficiency
0.493	0.026	0.020	0.008	20	0.380	1.E+06	15	0.103	4738	502	2251	99.26%
0.466	0.029	0.016	0.008	20	0.380	1.E+06	20	0.078	8127	351	2169	98.95%
0.472	0.033	0.015	0.008	20	0.380	1.E+06	25	0.060	13309	628	1771	98.45%
0.522	0.030	0.012	0.007	20	0.340	1.E+06	30	0.065	22379	688	1514	97.60%
0.522	0.030	0.012	0.007	20	0.340	1.E+06	35	0.052	35065	523	1211	96.45%
0.517	0.032	0.012	0.008	20	0.348	1.E+06	40	0.039	62417	847	902	93.97%
0.506	0.031	0.020	0.013	18	0.375	2.E+06	15	0.201	5976	773	3970	99.47%
0.506	0.033	0.020	0.010	17	0.380	2.E+06	20	0.138	8842	676	3615	99.35%
0.476	0.028	0.019	0.008	19	0.380	2.E+06	25	0.127	13355	622	3195	99.15%
0.465	0.030	0.016	0.008	20	0.380	2.E+06	30	0.116	18022	499	3187	98.93%
0.468	0.029	0.015	0.008	20	0.380	2.E+06	35	0.095	24085	1120	2822	98.62%
0.472	0.033	0.015	0.008	20	0.380	2.E+06	40	0.083	32984	1309	2442	98.20%
0.460	0.030	0.017	0.006	20	0.380	2.E+06	45	0.070	45911	1209	2017	97.60%
0.484	0.031	0.019	0.015	19	0.375	3.E+06	15	0.338	8256	993	5506	99.51%
0.505	0.032	0.020	0.012	17	0.380	3.E+06	20	0.215	10366	974	5175	99.45%
0.505	0.032	0.020	0.012	17	0.380	3.E+06	25	0.165	15586	729	3953	99.33%
0.465	0.028	0.019	0.008	19	0.380	3.E+06	30	0.169	19918	822	4291	99.17%
0.467	0.027	0.015	0.008	20	0.380	3.E+06	35	0.155	25681	726	4548	98.98%
0.468	0.029	0.015	0.008	20	0.380	3.E+06	40	0.135	31604	1587	4014	98.78%
0.465	0.030	0.016	0.008	20	0.380	3.E+06	45	0.116	41425	1990	3192	98.47%
0.484	0.031	0.019	0.015	19	0.375	4.E+06	15	0.463	9918	1364	7554	99.53%
0.505	0.032	0.020	0.012	17	0.380	4.E+06	20	0.300	11776	1360	7212	99.49%
0.505	0.032	0.020	0.012	17	0.380	4.E+06	25	0.232	16572	1036	5583	99.42%
0.512	0.025	0.017	0.012	18	0.380	4.E+06	30	0.203	22838	929	5003	99.29%
0.507	0.026	0.017	0.009	18	0.380	4.E+06	35	0.179	28565	892	4958	99.15%
0.467	0.027	0.015	0.008	20	0.380	4.E+06	40	0.187	35017	864	5476	98.98%
0.468	0.029	0.015	0.008	20	0.380	4.E+06	45	0.165	42944	1884	4791	98.77%
0.484	0.031	0.019	0.015	19	0.375	5.E+06	15	0.589	11641	1735	9603	99.54%
0.505	0.032	0.020	0.012	17	0.380	5.E+06	20	0.385	13361	1746	9250	99.52%
0.505	0.032	0.020	0.012	17	0.380	5.E+06	25	0.300	18081	1343	7213	99.47%
0.505	0.032	0.020	0.012	17	0.380	5.E+06	30	0.244	25367	1068	5858	99.36%
0.508	0.025	0.017	0.009	18	0.380	5.E+06	35	0.233	30738	1182	6486	99.24%
0.507	0.027	0.017	0.009	18	0.380	5.E+06	40	0.200	38541	974	5602	99.11%
0.478	0.031	0.018	0.008	18	0.380	5.E+06	45	0.180	46694	2207	5063	98.93%

Table 10 100 m/s Rotor Tip Speed HEMM 3000 RPM Design Tool Results

Rotor Back Iron Thickness Ratio	Rotor Iron Tooth Width (m)	Stator Back Iron Thickness (m)	Stator Winding Radial Thickness (m)	Rotor Pole Pair Count	Rotor Radius (m)	Power (W)	Specific Power (kW/kg)	Stack Length (m)	Winding Resistive Loss (W)	Winding Eddy Current Loss (W)	Stator Iron Losses (W)	Efficiency
0.483	0.028	0.015	0.010	17	0.320	1.0E+06	15	0.123	6484.2721	293.58763	2007.4383	99.13%
0.492	0.030	0.015	0.008	17	0.321	1.0E+06	20	0.093	11353	235	1815	98.68%
0.478	0.030	0.013	0.007	19	0.321	1.0E+06	25	0.088	17567	718	1557	98.05%
0.478	0.030	0.013	0.007	19	0.321	1.0E+06	30	0.069	26416	542	1224	97.26%
0.507	0.032	0.010	0.007	19	0.320	1.0E+06	35	0.060	40225	1001	1179	95.93%
0.507	0.032	0.010	0.007	19	0.320	1.0E+06	40	0.049	62540	754	967	93.96%
0.476	0.028	0.020	0.011	14	0.321	2.0E+06	15	0.208	7516	644	3578	99.42%
0.483	0.028	0.019	0.010	14	0.319	2.0E+06	20	0.153	13143	451	2746	99.19%
0.460	0.030	0.016	0.008	16	0.321	2.0E+06	25	0.150	18419	1060	2910	98.89%
0.460	0.030	0.016	0.008	16	0.321	2.0E+06	30	0.119	25475	1298	2326	98.57%
0.492	0.030	0.015	0.008	17	0.321	2.0E+06	35	0.111	34739	1107	2158	98.14%
0.492	0.030	0.015	0.008	17	0.321	2.0E+06	40	0.093	50133	875	1809	97.43%
0.510	0.032	0.013	0.007	18	0.320	2.0E+06	45	0.094	64609	1822	1863	96.70%
0.493	0.028	0.018	0.019	12	0.321	3.0E+06	15	0.255	10449	612	4342	99.49%
0.483	0.028	0.019	0.010	14	0.319	3.0E+06	20	0.247	14463	736	4440	99.35%
0.481	0.028	0.019	0.011	14	0.321	3.0E+06	25	0.187	21599	549	3405	99.16%
0.481	0.028	0.019	0.011	14	0.321	3.0E+06	30	0.149	29623	1138	2729	98.90%
0.460	0.030	0.016	0.008	16	0.321	3.0E+06	35	0.162	36267	1744	3166	98.65%
0.460	0.030	0.016	0.008	16	0.321	3.0E+06	40	0.138	49627	1408	2681	98.24%
0.492	0.030	0.015	0.008	17	0.321	3.0E+06	45	0.134	64994	1251	2599	97.76%
0.493	0.028	0.018	0.019	12	0.321	4.0E+06	15	0.357	11571	860	6078	99.54%
0.482	0.034	0.020	0.017	12	0.313	4.0E+06	20	0.266	18655	609	4280	99.41%
0.481	0.028	0.019	0.011	14	0.321	4.0E+06	25	0.261	23995	774	4764	99.27%
0.481	0.028	0.019	0.011	14	0.321	4.0E+06	30	0.212	30764	1634	3861	99.10%
0.460	0.030	0.016	0.008	16	0.321	4.0E+06	35	0.227	40858	1559	4423	98.84%
0.460	0.030	0.016	0.008	16	0.321	4.0E+06	40	0.195	51901	2024	3775	98.58%
0.460	0.030	0.016	0.008	16	0.321	4.0E+06	45	0.170	68777	1683	3292	98.19%
0.493	0.028	0.018	0.019	12	0.321	5.0E+06	15	0.459	12933	1108	7815	99.56%
0.482	0.034	0.020	0.017	12	0.313	5.0E+06	20	0.344	20572	790	5528	99.47%
0.481	0.028	0.019	0.011	14	0.321	5.0E+06	25	0.336	26848	999	6122	99.33%
0.481	0.028	0.019	0.011	14	0.321	5.0E+06	30	0.274	34868	793	4993	99.19%
0.483	0.028	0.019	0.010	14	0.319	5.0E+06	35	0.234	45775	1730	4207	98.98%
0.460	0.030	0.016	0.008	16	0.321	5.0E+06	40	0.251	56074	2639	4869	98.74%
0.460	0.030	0.016	0.008	16	0.321	5.0E+06	45	0.220	72600	2219	4266	98.44%

Table 11 80 m/s Rotor Tip Speed HEMM 3000 RPM Design Tool Results

Rotor Back Iron Thickness Ratio	Rotor Iron Tooth Width (m)	Stator Back Iron Thickness (m)	Stator Winding Radial Thickness (m)	Rotor Pole Pair Count	Rotor Radius (m)	Power (W)	Specific Power (kW/kg)	Stack Length (m)	Winding Resistive Loss (W)	Winding Eddy Current Loss (W)	Stator Iron Losses (W)	Efficiency
0.460	0.028	0.015	0.008	13	0.252	1.E+06	15	0.147	10133	504	1577	98.79%
0.480	0.028	0.013	0.008	14	0.252	1.E+06	20	0.120	17887	555	1334	98.06%
0.480	0.028	0.013	0.008	14	0.252	1.E+06	25	0.091	28171	398	1012	97.13%
0.480	0.028	0.013	0.008	14	0.252	1.E+06	30	0.072	47553	729	793	95.32%
0.502	0.029	0.009	0.007	16	0.248	1.E+06	35	0.085	72581	2226	856	92.97%
0.486	0.028	0.017	0.009	12	0.250	2.E+06	15	0.286	13749	384	3013	99.15%
0.475	0.028	0.017	0.009	12	0.250	2.E+06	20	0.207	21434	1122	2113	98.78%
0.466	0.028	0.015	0.008	13	0.252	2.E+06	25	0.183	31374	938	2015	98.31%
0.466	0.028	0.015	0.008	13	0.252	2.E+06	30	0.148	45761	718	1633	97.65%
0.480	0.028	0.013	0.008	14	0.252	2.E+06	35	0.141	64830	1480	1562	96.72%
0.480	0.028	0.013	0.008	14	0.252	2.E+06	40	0.120	86409	3044	1333	95.66%
0.528	0.031	0.017	0.015	11	0.250	3.E+06	15	0.367	18770	410	3426	99.25%
0.475	0.028	0.017	0.009	12	0.250	3.E+06	20	0.324	26695	1124	3312	98.97%
0.486	0.028	0.017	0.009	12	0.250	3.E+06	25	0.254	37853	1343	2670	98.62%
0.466	0.028	0.015	0.008	13	0.252	3.E+06	30	0.236	51210	1173	2593	98.20%
0.466	0.028	0.015	0.008	13	0.252	3.E+06	35	0.198	71359	2379	2172	97.53%
0.466	0.028	0.015	0.008	13	0.252	3.E+06	40	0.170	94277	1898	1867	96.84%
0.522	0.030	0.019	0.017	10	0.247	4.E+06	15	0.444	22034	1297	3913	99.32%
0.528	0.031	0.017	0.015	11	0.250	4.E+06	20	0.367	31857	1683	3430	99.08%
0.486	0.028	0.017	0.009	12	0.250	4.E+06	25	0.346	44291	1841	3568	98.77%
0.466	0.028	0.015	0.008	13	0.252	4.E+06	30	0.323	58830	1627	3554	98.42%
0.466	0.028	0.015	0.008	13	0.252	4.E+06	35	0.273	80309	3344	2992	97.88%
0.466	0.028	0.015	0.008	13	0.252	4.E+06	40	0.236	103503	2709	2585	97.35%
0.480	0.028	0.013	0.008	14	0.252	4.E+06	45	0.233	134185	6009	2591	96.55%
0.522	0.030	0.019	0.017	10	0.247	5.E+06	15	0.565	26415	615	4967	99.36%
0.522	0.030	0.019	0.017	10	0.247	5.E+06	20	0.414	37754	1808	3621	99.14%
0.486	0.028	0.017	0.009	12	0.250	5.E+06	25	0.437	51017	2351	4468	98.86%
0.478	0.028	0.017	0.008	12	0.250	5.E+06	30	0.365	68313	1888	3842	98.54%
0.475	0.028	0.017	0.009	12	0.250	5.E+06	35	0.307	90117	3752	3114	98.10%
0.465	0.028	0.015	0.008	13	0.252	5.E+06	40	0.299	117242	3489	3182	97.58%
0.464	0.028	0.015	0.008	13	0.252	5.E+06	45	0.263	144975	7534	2804	96.99%

Acknowledgments

This work was supported by the Electrified Aircraft Powertrain Technologies Subproject within the Advanced Air Transport Technology Project of NASA's Aeronautics Research Mission Directorate. Additional support was provided by the Convergent Aeronautics Solutions Project of NASA's Aeronautics Research Mission Directorate.

References

[1] C. A. Luongo, P. J. Masson, T. Nam, D. Mavris, H. D. Kim, G. V. Brown, M. Waters and D. Hall, "Next Generation More-Electric Aircraft: A Potential Application for HTS Superconductors," *IEEE TRANSACTIONS ON APPLIED SUPERCONDUCTIVITY,* vol. 19, no. 3, 2009.

[2] P. J. Masson, G. V. Brown, D. S. Soban and C. A. Luongo, "HTS machines as enabling technology for all-electric airborne vehicles," *Superconductor Science and Technology,* vol. 20, no. 8, 2007.

[3] J. Tangudu, Z. Tao and P. Kshirsagar, "Analytical Model and Design Space Studies a Studies a Superconducting Machine for an Aircraft Application," in *AIAA/IEEE Electric Aircraft Technologies Symposium* , Virtual, 2020.

[4] Y. Terao, Y. Ishida, D. Heideman, H. Ohsaki, K. Okai and H. Taguchi, "Electromagnetic Analysis of Fully Superconducting Synchronous Machines for Future Turbo Electric Propulsion Systems," in *AIAA/IEEE Electrified Aircraft Tehcnology Symposium* , Virtual, 2020.

[5] J. Voccio, J. Tangudu and B. Wawrzyniak, "Design and Evaluation of a High Power Density 5 MW, 6000 RPM Fully-superconducting Generator," in *Electric Aircraft Tehcnologies Symposium*, Virtual, 2020.

[6] T. Balachandran, J. Rebandi, J. Xiao, S. Srimmana and K. Haran, "Co-design of an Integrated Direct-drive Electric Motor and Propeller for Aircraft Propulsion," in *AIAA/IEEE Electric Aircraft Technologies Symposium*, 2020.

[7] K. P. Duffy, P. J. Passe, R. W. Dyson and R. H. Jansen, "Design Analysis and Testing of the HEMM Cryocooler Linear Motor," in *AIAA/IEEE Electrified Aircraft Technologies Symposium*, New Orleans, 2020.

[8] R. W. Dyson, R. H. Jansen, K. P. Duffy and P. J. Passe, "High Efficiency Megawatt Machine Rotating Cryocooler Conceptual Design," in *AIAA Propulsion and Energy Forum*, Indianapolis, 2019.

[9] R. H. Jansen, Y. De Jesus-Arce, P. Kascak, R. Dyson, A. Woodworth, J. J. Sheidler, R. Edwards, E. Stalcup, J. Whilhite, K. Duffy, P. Passe and S. McCormick, "High Efficiency Megawatt Motor Conceptual Design," in *AIAA Propulsion and Energy Forum*, Cincinnati, 2018.

[10] R. H. Jansen, P. Kascak, R. Dyson, A. Woodworth, J. Scheidler, A. D. Smith, T. Tallerico, Y. De Jesus-Arce, D. Avanesian, K. Duffy, P. Passe and G. Szpak, "High Efficiency Megawatt Motor Preliminary Design," in *AIAA/IEEE Electric Aircraft Technologies Synmposium*, Indianapolis, 2019.

[11] G. Sapak, A. Smith, J. T. Thompson, A. Woodworth and R. Jansen, "High Efficiency Megawatt Motor Thermal Stator Preliminary Design," in *AIAA/IEEE Electrified Aircraft Technologies Symposium*, New Orleans, 2020.

[12] J. J. Scheidler, "Preliminary Design of the Superconducting Rotor for NASA's High-Efficiency Megawatt Motor," in *AIAA Propulsion and Energy Forum*, Cincinnati, 2018.

[13] J. J. Scheidler and T. F. Tallerico, "Design, Fabrication, and Critical Current Testing of No-Insulation Superconducting Rotor Coils for NASA's 1.4 MW High-Efficiency Megawatt Motor," in *AIAA/IEEE Electric Aircraft Technologies Symposium*, Cincinnati, 2018.

[14] J. J. Sheidler, T. F. Tallerico, W. A. Miller and W. Torres, "Progress Toward the Critical Design of the Superconducting Rotor for NASA's 1.3 MW High-Efficiency Electric Machine," in *AIAA/IEEE Electric Aircraft Technologies Symposium*, Indianapolis, 2019.

[15] T. Tallerico, J. Scheidler, D. Lee and K. Haran, "Electromagnetic Redesign of NASA's High Efficiency Megawatt Motor," in *AIAA/IEEE Electric Aircraft Technologies Symposium*, Virtual, 2020.

[16] J. R. Welstead and J. L. Felder, "Conceptual Design of a Single-Aisle Tuboelectric Commercial Transport with Fuselage Boundary Layer Ingestion," in *AIAA SciTech 2016*, San Diego, 2016.

[17] A. A. Woodworth, R. Jansen, K. Duffy, P. Nazhipour and E. Shin, "Creating a Multifunctional Composite Stator Slot Material System to Enable High Power Density Electric Machines for Electrified Aircraft Applications," in *AIAA/IEEE Electric Aircraft Technologies Symposium*, Cincinnati, 2018.

[18] V. Venkatachalam, C. Sullivan, T. Abdallah and H. Tacca, "Accurate Predicition of Ferritie Core Loss with Non-Sinusoidal Waveforms Using only Steinmets Parameters," in *Computers in Power Electronics* , Mayaguez, 2002.

[19] National Electrical Manufacturers Association, "NEMA MW 1000-2003," National Electrical Manufacturers Association, Rosslyn, VA, 2003.

[20] R. H. Jansen, G. V. Brown, J. L. Felder and K. P. Duffy, "Turboelectric Aircraft Drive Key Performance Parameters and Functional Requirments," in *AIAA Propusion and Energy Forum*, Orlando, 2015.

[21] A. A. Woodworth, A. Smith, W. Sixel, R. Edwards, R. Jansen, S. McCormick, M. Robbie, G. Szpak, P. Naghipour and E.-S. Shin, "Thermal Analysis of Potted Litz Wire for High-Power-Density Aerospace Electric Machines," in *AIAA Propulsion and Energy Forum*, Indianapolis, 2019.

[22] R. H. Jansen, J. Scheidler, T. Tallerico, P. Kascak, A. Woodworth, A. Smith, R. Dyson, W. Sixel, J. Thompson, E. Stalcup, Y. De Jesus-Acre, D. Avanesian, K. Duffy, P. Passe and G. Szpak, "High Efficiency Megawatt Motor Risk Reduction Activities," in *Electrified Aircraft Technologies Symposium*, New Orleans, 2020.